Advanced CUBIC tissue clearing for whole-organ cell profiling

Katsuhiko Matsumoto[1,10], Tomoki T. Mitani[1,2,3,10], Shuhei A. Horiguchi[1,4,10], Junichi Kaneshiro[5], Tatsuya C. Murakami[6], Tomoyuki Mano[7,8], Hiroshi Fujishima[1], Ayumu Konno[9], Tomonobu M. Watanabe[5], Hirokazu Hirai[9] and Hiroki R. Ueda[1,6,7,8*]

Tissue-clearing techniques are powerful tools for biological research and pathological diagnosis. Here, we describe advanced clear, unobstructed brain imaging cocktails and computational analysis (CUBIC) procedures that can be applied to biomedical research. This protocol enables preparation of high-transparency organs that retain fluorescent protein signals within 7–21 d by immersion in CUBIC reagents. A transparent mouse organ can then be imaged by a high-speed imaging system (>0.5 TB/h/color). In addition, to improve the understanding and simplify handling of the data, the positions of all detected cells in an organ (3–12 GB) can be extracted from a large image dataset (2.5–14 TB) within 3–12 h. As an example of how the protocol can be used, we counted the number of cells in an adult whole mouse brain and other distinct anatomical regions and determined the number of cells transduced with mCherry following whole-brain infection with adeno-associated virus (AAV)-PHP.eB. The improved throughput offered by this protocol allows analysis of numerous samples (e.g., >100 mouse brains per study), providing a platform for next-generation biomedical research.

Introduction

Tissue-clearing techniques and high-resolution volumetric imaging by light-sheet fluorescence microscopy[1–4] with appropriate fluorescent labeling can provide comprehensive cell information such as cell type, shape, state and distribution of cells of interest throughout an organ. In particular, tissue-clearing techniques combined with light-sheet fluorescence microscopy are a powerful tool to quantify rare cells such as stem cells, metastatic cells or activated neurons in a whole organ for biological research and pathological diagnosis[5–9]. Furthermore, advancing biomedical research requires numerous experiments and verifications; thus a simple high-throughput and stable protocol is important to facilitating comprehensive whole-organ cell profiling. Here, we describe a whole-organ cell profiling pipeline that includes advanced tissue-clearing methods, use of a novel high-speed volumetric imaging system with a customized light-sheet fluorescence microscope (LSFM) and a high-speed cell-nucleus-detection algorithm (Fig. 1). We have previously used this protocol to create transparent whole mouse organs or human organ blocks[10], as well as whole-brain cell profiling of mice from 1 week old to 8 weeks old, demonstrating substantial changes in cell numbers in particular areas during postnatal development[11].

Tissue-clearing methods

To prepare a transparent organ for volumetric imaging, three major approaches have been reported: hydrophobic, hydrophilic and hydrogel-based tissue-clearing methods. Hydrophobic tissue-clearing methods (e.g., BABB, 3DISCO, uDISCO, iDISCO)[4,12–15] lead to high-transparency organs within a few days. However, some organic solvents require careful handling[14,] and the cleared organ will shrink, which is a disadvantage for high-resolution imaging. Hydrogel-based methods (e.g., CLARITY)[16] provide high-transparency organs within a week, but it is difficult to apply to many

[1]Laboratory for Synthetic Biology, RIKEN Center for Biosystems Dynamics Research, Osaka, Japan. [2]Faculty of Medicine, Osaka University, Osaka, Japan. [3]Osaka University Hospital, Osaka, Japan. [4]Department of Electrical Engineering and Information Systems, Graduate School of Engineering, The University of Tokyo, Tokyo, Japan. [5]Laboratory for Comprehensive Bioimaging, RIKEN Center for Biosystems Dynamics Research, Osaka, Japan. [6]Department of Systems Pharmacology, Graduate School of Medicine, The University of Tokyo, Tokyo, Japan. [7]Department of Information Physics and Computing, Graduate School of Information Science and Technology, The University of Tokyo, Tokyo, Japan. [8]International Research Center for Neurointelligence (WPI-IRCN), UTIAS, The University of Tokyo, Tokyo, Japan. [9]Department of Neurophysiology & Neural Repair, Gunma University Graduate School of Medicine, Maebashi, Japan. [10]These authors contributed equally: Katsuhiko Matsumoto, Tomoki T. Mitani, Shuhei A. Horiguchi. *e-mail: uedah-tky@umin.ac.jp
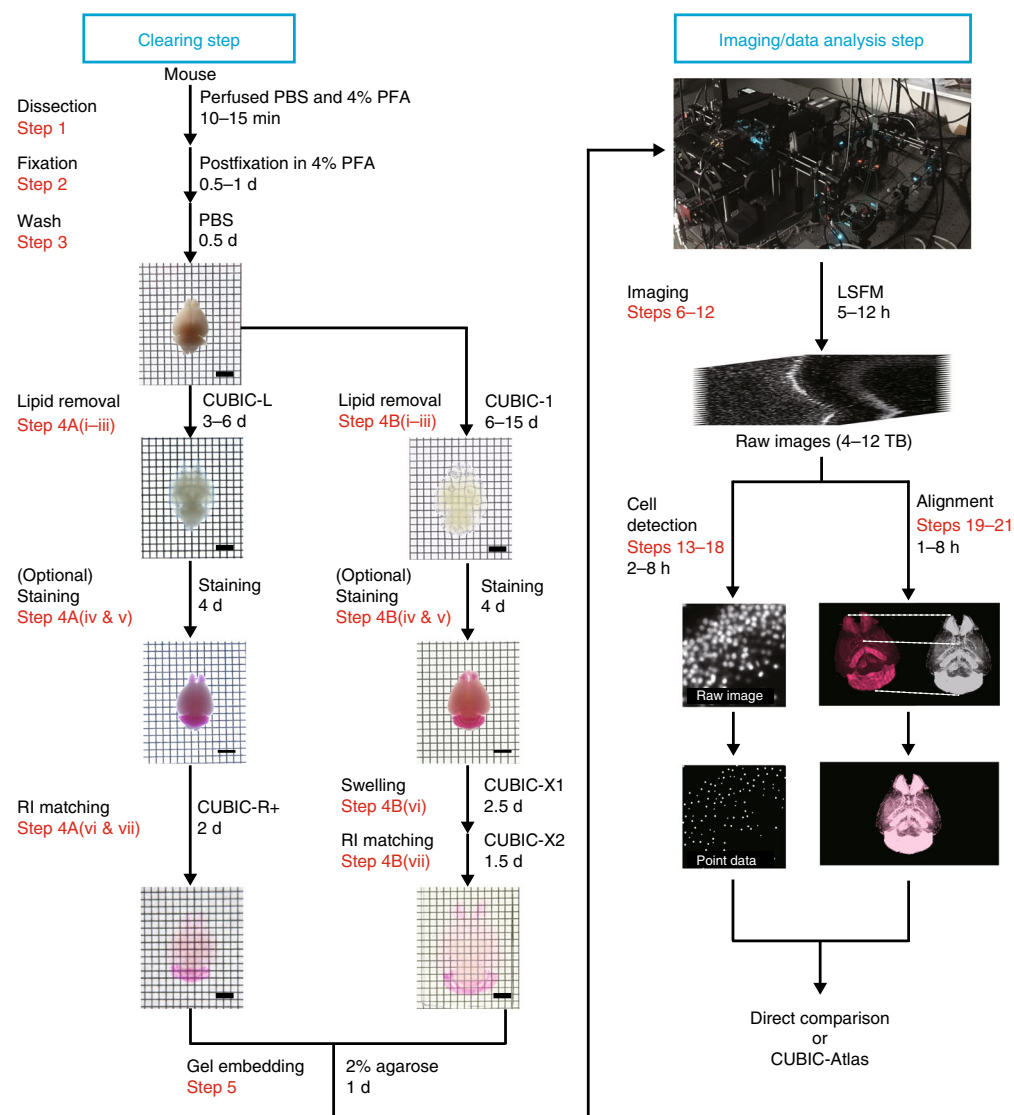
Fig. 1 | Overview of the advanced CUBIC pipeline in whole-organ cell profiling. This pipeline comprises three major stages (tissue clearing, imaging and image analysis). We provide two kinds of clearing protocols: a rapid and high-quality protocol using CUBIC-L and CUBIC-R+ (Step 4A), which takes at least 7 d for adult mouse brain, and a tissue expansion protocol for high-resolution imaging using CUBIC-X (Step 4B), which takes up to 21 d for adult mouse brain. In addition, both protocols can include staining with an appropriate nuclei-staining dye, which takes 4 d. Rapid volumetric imaging can be performed with a customized LSFM with the MOVIE system (Steps 6–12). From the collected volumetric images, cells are detected by GPUs and CPUs and converted to point data. When analyzing the mouse brain, the result data are analyzed with CUBIC-Atlas. Scale bars, 5 mm. All experiments followed the relevant governmental and institutional guidelines for animal experiments.

samples without dedicated equipment for electrophoresis. In addition, acrylamide has been reported to be carcinogenic and toxic in the liquid state[17]. To overcome these disadvantages, the passive clarity technique (PACT)[18,19] for parallel handling and acrylamide-free methods such as SHIELD[20], which uses a safer flexible polyepoxide instead of acrylamide for hydrogel formation, has been developed. Hydrophilic tissue-clearing methods using X-ray contrast agents, sugars or PEG were first described by the Tuchin group[21–24] and have led to the development of other hydrophilic tissue-clearing methods (e.g., CUBIC, Sca*l*e and SeeDB)[25–29]. Desirable attributes for tissue-clearing techniques in routine biomedical research are safety, simple operation, scalability, low environmental burden and high transparency. Hydrophilic tissue-clearing approaches have the potential to fulfil all of these requirements. CUBIC reagents that are based on hydrophilic reagents have been developed to prioritize safety and decrease environmental burden, and these protocols require only sample immersion in clearing media, in order to minimize the number of experimental procedures and to
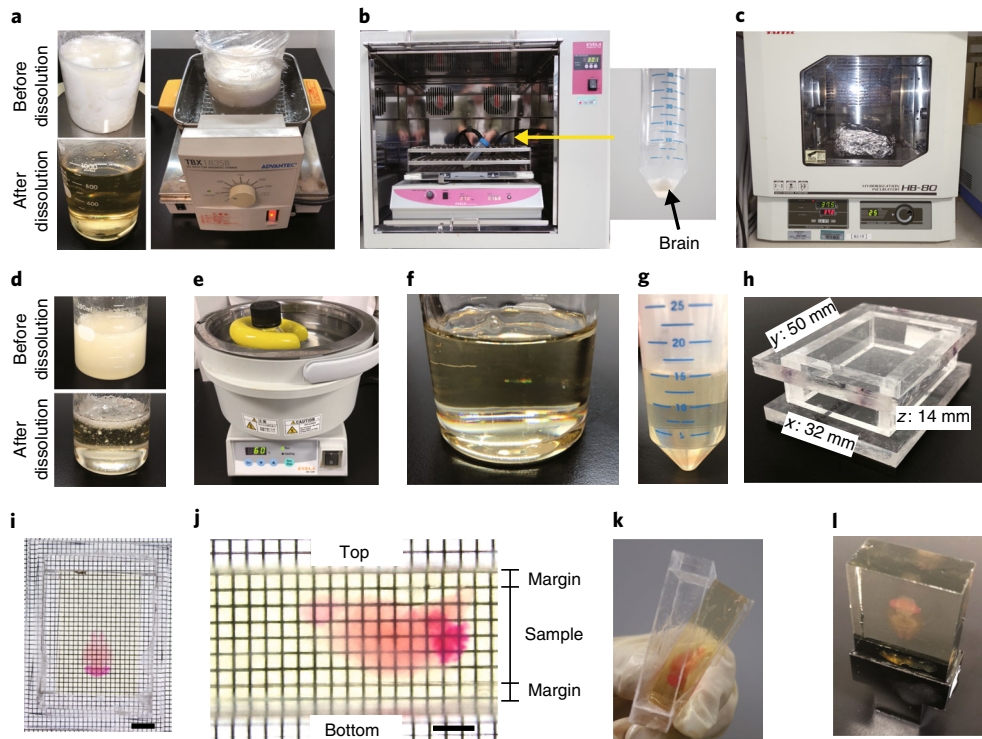
Fig. 2 | Procedures for tissue clearing and gel embedding. a, Preparation of CUBIC-R+. This reagent can be easily dissolved by mild heating and stirring. **b,c**, An incubator with a shaker (**b**) and a hybridization incubator (**c**) that we use for steps requiring temperature control for the clearing procedure; inset shows tube containing brain. **d**, Preparation of 2% agarose–CUBIC solution. Agarose can be dissolved by repeated heating using a microwave and shaking. **e**, A water bath for the degassing step. **f**, 2% agarose–CUBIC solution after the degassing step. **g**, The sample is immersed in 2% agarose–CUBIC solution before gelation. **h**, A mold for gelation. It is designed for mouse brain. **i**, x–y view after gelation. Scale bar, 10 mm. **j**, y–z view after gelation. Scale bar, 5 mm. A margin of 1 mm or more is recommended on the top and bottom of the sample. **k**, Removing the sample gel from the mold. **l**, Fixation of the gel on the customized sample holder. All experiments followed the relevant governmental and institutional guidelines for animal experiments.

enable easy handling of multiple samples. An additional advantage of the CUBIC reagents is that amino alcohols are able to decolor endogenous heme in mouse whole-organ and whole-body samples[27,30]. Since CUBIC reagents were first reported, the reagents and protocols have been continuously updated to improve the transparency and to reduce the handling time[10,11]. In the present protocol, we describe two types of whole-organ clearing procedures: the latest (to our knowledge) protocol for rapid and high-quality organ clearing using CUBIC-L and CUBIC-R+ (Step 4A) and the tissue expansion–based CUBIC-X protocol for high-resolution imaging (Step 4B). These procedures are applicable to a whole mouse brain of any strain, age and sex. To apply them to other mouse organs or organisms, users may need to make some modifications to the procedure, such as changing reagent volumes and immersion durations. The details are described below (Fig. 2 and Steps 1–5).

Methods of volumetric imaging

Historically, imaging technologies have been critical to advancing biomedical research and, recently, it has become important to be able to image whole organs with single-cell resolution. Almost all biomedical research requires analysis of numerous samples; therefore, increasing imaging throughput is essential to research efficiency. Confocal microscopy and multiphoton-excitation fluorescence microscopy are often used to obtain volumetric images. However, in general, the imaging speed is not suitable for large specimens such as a whole adult mouse brain[31–33]. Therefore, destructive methods such as serial-sectioning-based tomography or confocal microscopy are used for volumetric imaging. For example, a high-speed serial-sectioning imaging system (FAST) that enabled imaging of a whole mouse brain in 2 h and 24 min was reported[34]. However, such destructive methods destroy the sample and

prevent users from being able to reanalyze the samples. Light-sheet fluorescence microscopy can be used to non-destructively obtain volumetric images of the intact transparent organ because imaging throughput is high and the light and physical damage is lower than that of any other imaging methods[3,35]. Using the homogeneous 2.2-fold expansion protocol (CUBIC-X) and a customized LSFM equipped with a 10× objective lens, we previously succeeded in high-resolution imaging of a whole mouse brain (amounting to 14 TB of data) from which all the cell nuclei were detected and analyzed[11]. However, this imaging speed cannot be applied to many samples because the image acquisition of the expanded whole mouse brain required 4 d. To overcome this challenge, we developed the moving observation with efficient real-time autofocus (MOVIE) system for efficient volumetric imaging, which integrates (i) continuous acquisition (MOVIE-scan), (ii) real-time autofocusing (MOVIE-focus) and (iii) skipping of blank images (MOVIE-skip). Consequently, imaging throughput was increased by five to eight times. The details are described below ('Whole-organ imaging' and 'MOVIE advanced high-speed imaging system' in 'Experimental design', Figs. 3–6 and Steps 6–12).

Cell-nucleus-detection algorithm

In parallel with the rapid technological advancements in volumetric imaging, informatics tools have also been improved. In recent years, whole-organ-scale analysis of mammals, fish or flies has been developed[2,11,15,27,30,36–42]. For cellular-resolution volumetric images, segmentation of cell bodies or nuclei has been attempted in many studies[5,41,43–52]. Various algorithms for blob (cell-nucleus) detection were reviewed by Xing and Yang in 2016 (ref. [53]). Most algorithms locate points of interest and then delineate the boundaries; however, our algorithm, which is based on the algorithm reported by Zhang et al.[54], performs the segmentation without locating points. We extended their algorithm in several places to make it applicable to 3D whole-organ images.

Here, we summarize three distinct challenges for blob detection in 3D whole-organ-scale images. First, touching or overlapping blobs are difficult to separate correctly. Three-dimensional images have another dimension in which blobs can be connected in more complex ways. Second, heterogeneity in morphology and brightness of blobs over a single organ prevent us from applying most of the simple algorithms. Heterogeneity in brightness could stem from congestion of blobs and decay of laser illumination intensity. Third, a massive number of images have to be processed in a short time for practical usage. In terms of effective utilization, the throughput of the informatics pipeline should be about the same as that of the volumetric imaging.

To overcome these challenges, we propose a cell-nucleus-detection algorithm based on 3D Hessian-based difference of Gaussian (3D-HDoG) with intensity normalization and have implemented a highly parallelized algorithm to utilize the parallel processing capabilities of multiple CPUs and graphics processing units (GPUs)[11,54]. In regard to accuracy, this algorithm attained an F score of >90% overall for the adult whole mouse brain cleared by the CUBIC-X protocol. It also achieved a >90% F score for the CUBIC-L/R+-treated adult whole mouse brain, except for the areas with extremely high cell densities, such as the olfactory bulb and cerebellum. Using a higher-magnification objective should improve the F score in areas with high cell density. Because CUBIC-X expands organs, it has consequences similar to those for increasing the magnification or using a thinner light sheet. Details of this cell-nucleus-detection algorithm are described below ('Cell-nucleus detection and annotation' in the 'Experimental design' section, Figs. 7,8 and Steps 13–21).

Experimental design
Overview of the advanced CUBIC pipeline

Here, we focus on describing (i) the rapid and highly transparent protocol (CUBIC L/R+; Step 4A) and tissue expansion protocol (CUBIC-X; Step 4B), (ii) high-throughput whole-organ imaging with a customized LSFM (Steps 6–12) and (iii) cell-nucleus detection using multiple GPUs and CPUs, and comparison between samples and annotation in single-cell resolution using CUBIC-Atlas (Steps 19–21) (Fig. 1).

Tissue clearing

Here, we provide two organ-clearing procedures: a rapid and high-performance CUBIC-L/R+ protocol (Step 4A) and a tissue expansion–based CUBIC-X protocol for high-resolution imaging (Step 4B). These procedures have been used previously[10,11], but more details are given here (Fig. 2a–c). Users should select appropriate clearing protocols for their research. The CUBIC-L/R+ protocol (Step 4A) is suitable for high-quality imaging, cell counting of low-cell-density organs or regions, or low-resolution
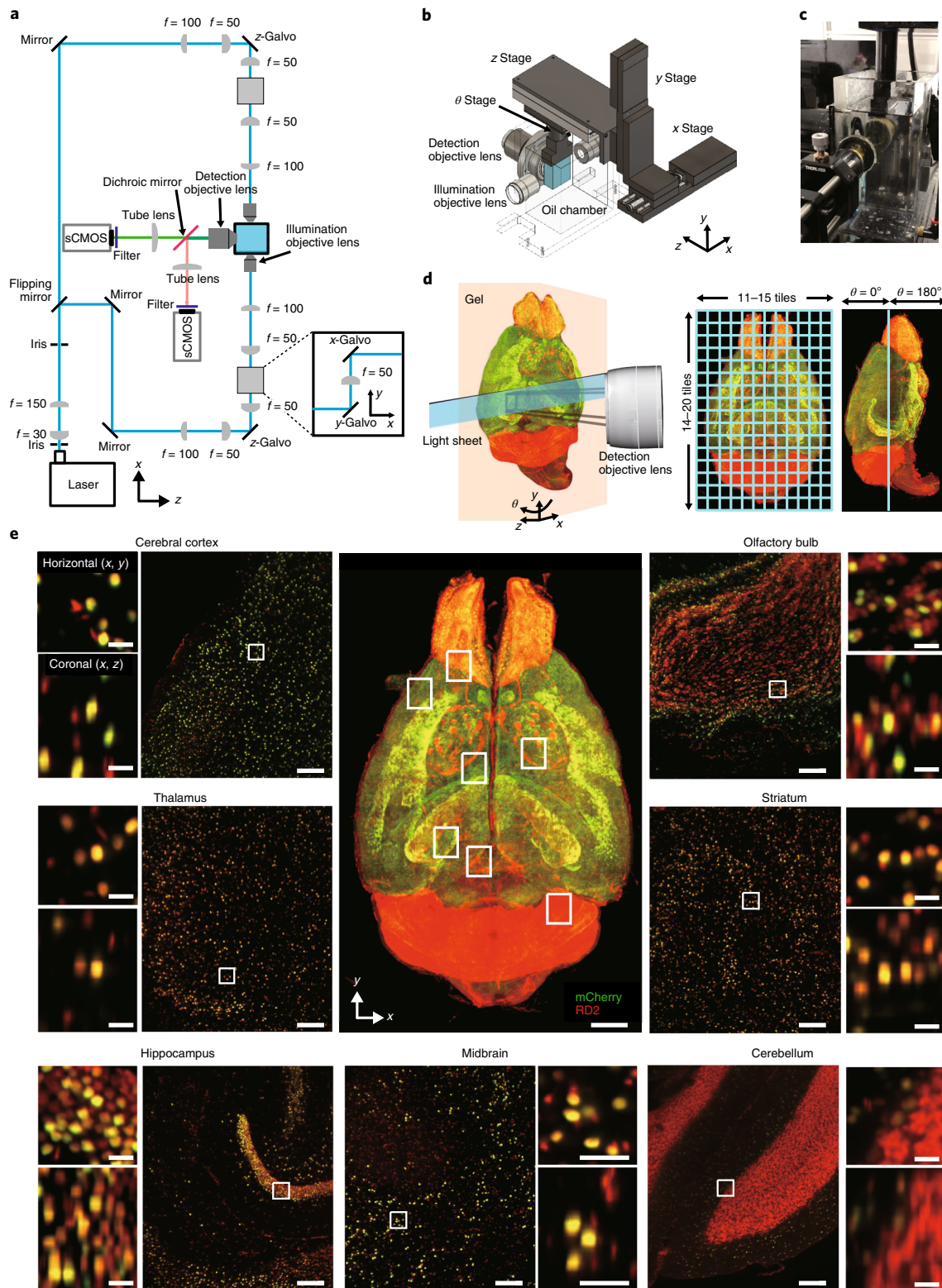
Fig. 3 | Whole-organ imaging with a customized LSFM. a, Schematic of a customized LSFM. **b**, Illustration of observation part of a customized LSFM. **c**, Picture of sample gel after installation on an LSFM. **d**, Procedure for imaging. Each stack of images is collected at the z range at a 7–7.5 mm thickness; 12 × 16 tiles (total 192 tiles) were acquired for half of a CUBIC-L/R+-treated mouse brain. After acquisition from the $\theta = 0°$ side, it automatically rotates and acquires the $\theta = 180°$ side. **e**, Volume-rendered and single-plane images of a brain transduced with AAV-PHP.eB:NSE-H2B-mCherry (mCherry, green) counterstained with RD2 (red), which is cleared by CUBIC-L/R+. Overlapped signals are shown in yellow. A volume-rendered image is shown in the center. Single-plane and magnified images are shown for cerebral cortex, thalamus, hippocampus, midbrain, cerebellum, olfactory bulb and striatum. Both horizontal (x–y) and coronal (x–z) views are also shown. Scale bars, 2 mm (3D image), 200 μm (single-plane images) and 25 μm (magnified images). All experiments followed the relevant governmental and institutional guidelines for animal experiments.
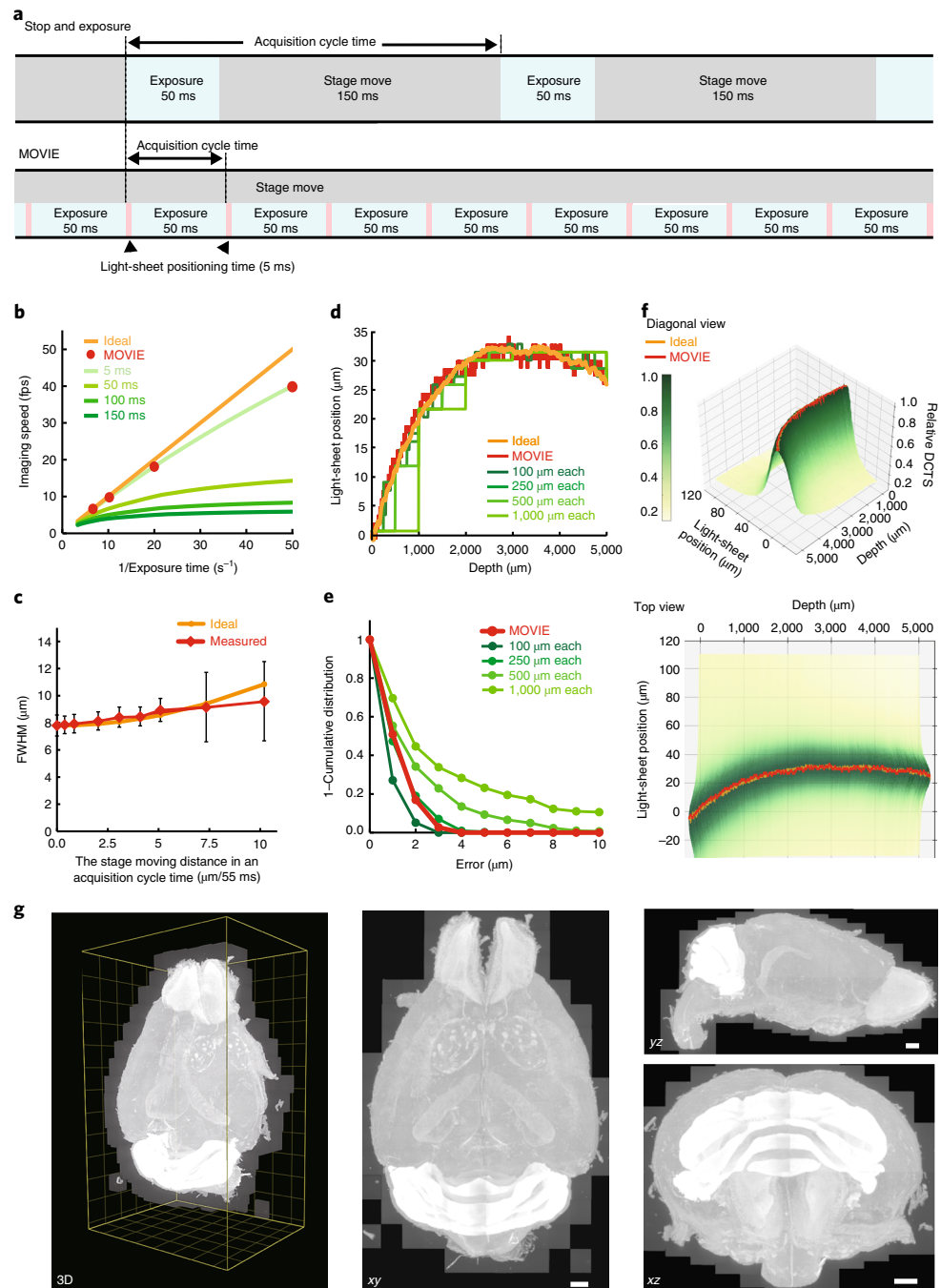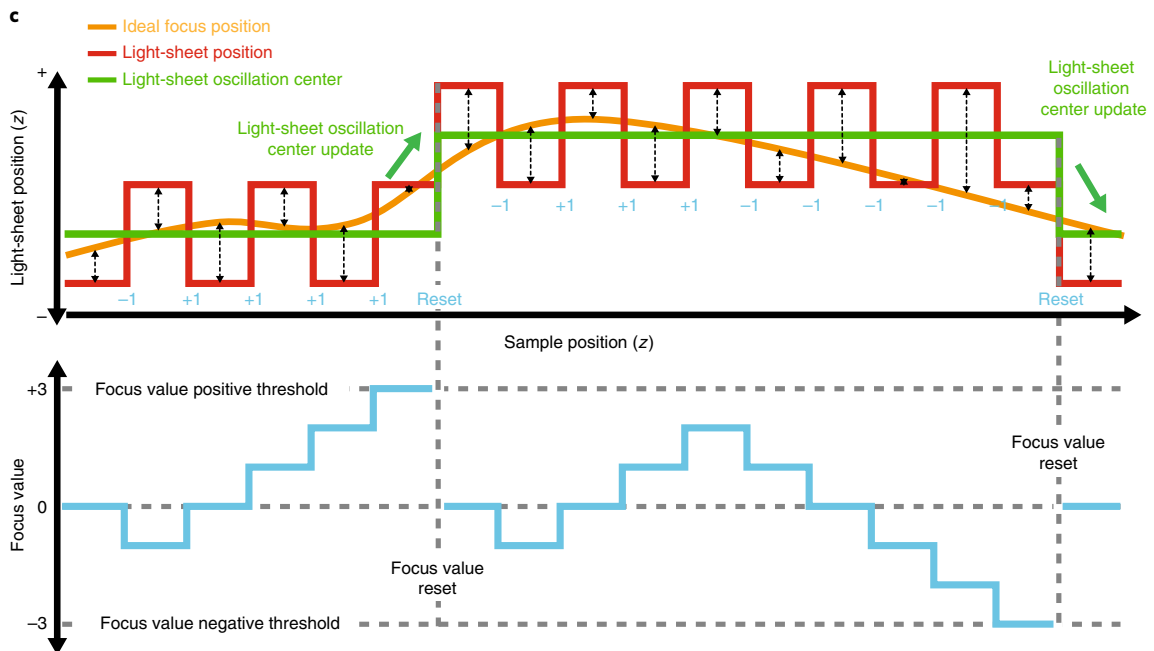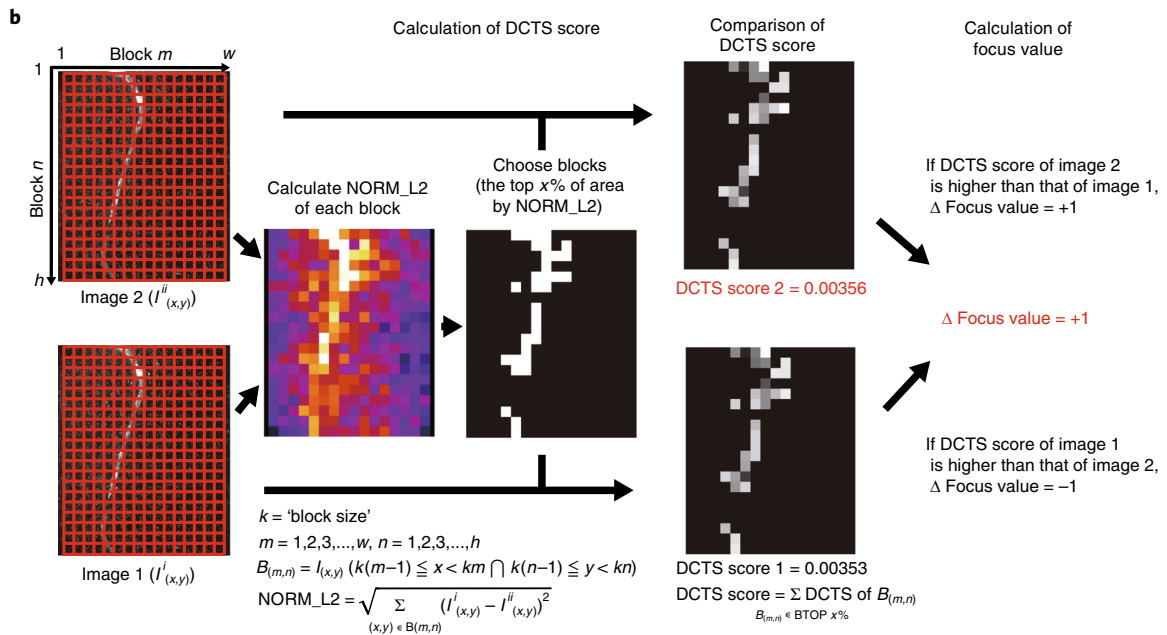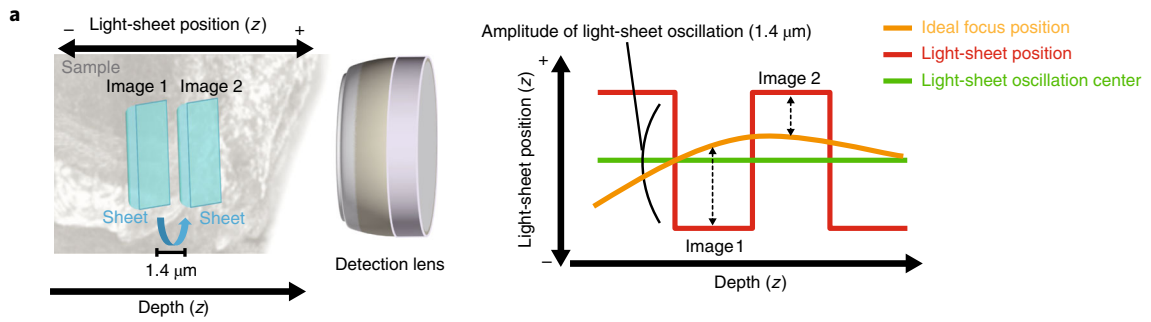
Fig. 4 | MOVIE system for high-speed and high-quality volumetric imaging. a, Imaging cycle of conventional stop-and-exposure method and MOVIE-scan method. Figure shows the case of a 50-ms exposure time. **b**, Imaging throughput with various stage positioning times. 'Ideal' shows an ideal case, in which an acquisition cycle time is equal to an exposure time. **c**, The axial FWHM (resolution along the z axis) of different MOVIE-scan speeds measured by acquiring images of fluorescent beads by light sheet with a 7.8-µm FWHM. 'Ideal' shows calculated FWHM of the light sheet. **d**, Simulation of MOVIE-focus and 'stop and exposure' autofocusing at 100, 250, 500 and 1,000 µm each. Ideal focus positions were calculated by DCTS metrics. **e**, Complementary cumulative distribution (1 − cumulative distribution) of error in MOVIE-focus and various 'stop and exposure' autofocus simulations. The error is defined as a distance between a simulated light-sheet position and an ideal focus position. **f**, 3D landscape of various autofocus simulations. Simulated points were illustrated by depth (µm), light-sheet position (µm) and relative DCTS (relative DCTS of an ideal focus position at each depth was defined as 1). The trajectory of MOVIE focus was described as orange line. **g**, Result of MOVIE-skip described by 3D images of PI-stained mouse brain. A region within the yellow frame (left) was acquired by the previous imaging algorithm. After MOVIE-skip, only the non-blank region was imaged (center and right-hand images). The number of images acquired with MOVIE-skip was decreased by 57% compared to the full, non-skipped images. Scale bars, 1 mm.

◀ **Fig. 5 | Details of MOVIE-focus. a**, Scheme of MOVIE-focus. During scan, images with oscillating light-sheet positions were acquired, and depending on the image quality metrics (as detailed in **b**), the light-sheet positions were continuously updated. Typically, the step size (i.e., amplitude) of the light-sheet oscillation was 1.4 μm. **b**, The scheme of image quality evaluation. To achieve real-time processing, we divided the images into blocks and selected the blocks with high NORM_L2 values. Typically, we divided a 2,160 × 2,560-pixel image into 128 × 128-pixel blocks ($k = 128$), resulting in 320 blocks, and selected the top 32 blocks (top 9.5% of image size, $x = 9.5$) by NORM_L2 values. The set of pixel indices (x,y) in the block (m,n) is denoted as $B_{(m,n)}$ and the set of selected blocks is denoted as 'BTOP' x%. Then, Shannon entropy of the normalized discrete cosine transform (DCTS) of each selected block was calculated, and the DCTS score was obtained by taking the summation of all selected blocks. Last, the DCTS scores of two images were compared, and the image with the higher DCTS score was chosen as the better focus direction, and 'focus value' was updated by +1 or −1, corresponding to the better focus direction. **c**, Real-time autofocus sequence in MOVIE-focus is shown. As the z-stack image scan proceeds, the light-sheet position was oscillated with a small step size (shown as red line). The image quality metrics of two images before and after the light-sheet position change were evaluated (as detailed in **b**), and the focus value was updated by either +1 or −1, corresponding to the better focus direction (shown as cyan line). Once the focus value crosses the threshold (in this figure, we use 3 or −3 as the threshold), the center of the light-sheet oscillation was updated ('focus update', shown as green arrows). After the update of a light-sheet position, the focus value was initialized to 0 and the autofocus sequence was repeated.

imaging for purposes such as screening. The CUBIC-X protocol (Step 4B) is suitable when images of high-cell-density organs or regions such as the cerebellum of the mouse brain are required.

Before application of CUBIC, animals are transcardially perfused with cold Dulbecco's PBS (D-PBS) and 4% paraformaldehyde (PFA) phosphate buffer solution and the organs are dissected for postfixation (Steps 1 and 2). After washing out the remaining PFA with PBS (Step 3), the fixed organs are treated with lipid-removal reagent (CUBIC-L) or a delipidation step. For the CUBIC-X protocol (Step 4B), the organs are treated with CUBIC-X1 solution for expansion. Finally, the refractive index (RI) of the organs is adjusted by CUBIC-R+ (Step 4A(vii)) or CUBIC-X2 (Step 4B(vii)). Both protocols can also stain the cell nucleus with an appropriate nuclear stain after the delipidation step (Table 1). This procedure can be paused at various points, which are indicated in the procedure.

Whole-organ imaging

We constructed a customized LSFM with a detection objective lens with a magnification of 10×, numerical aperture (NA) of 0.6, working distance (WD) of 8 mm and a pair of scientific CMOS cameras (Zyla 5.5, Andor) for whole-organ imaging (Fig. 3a–c). For fully automated imaging, the cleared organ is embedded in transparent agarose gel and fixed on the motorized x–y–z–θ stage. Gel embedding steps are shown in Fig. 2d–l, and these details are described below (Step 5A). Calibration gels including fluorescent beads (Step 5B) are used to calibrate the optical path of dual-color imaging and measure the point spread function (PSF). The field of view of our customized LSFM is 1.40 mm × 1.66 mm in the x–y plane, and the imaging region is divided into a grid, with a 0.13-mm overlap of each stack in both the x and y directions (Fig. 3d). In this customized LSFM, the beam waist was adjusted to ~10 μm so that consequent Rayleigh length was 0.53 mm at 594 nm, which corresponded to a uniform light-sheet thickness throughout the field of view in the immersion oil for CUBIC-X and CUBIC-R+. The full-width at half-maximum (FWHM) of the axial direction was measured as 7.8 μm by using PSFj[55]. We chose a scanning step size of 5 μm in the z direction, close to half the width of the beam waist. Because the WD of the detection objective lens determines the imaging range of the z direction, acquisition of the sample images is performed from two opposite directions, using a θ-stage rotation to collect images of the entire large specimen. For example, when an adult whole mouse brain with >10-mm thickness in the z axis is imaged, >5.5-mm stacks are imaged from the dorsal side, and the sample is then rotated by 180° and >5.5-mm stacks are imaged from the ventral side. Typically, we set a >0.5-mm overlap, but it depends on the verticality of the θ stage. We also demonstrated the simultaneous dual-color imaging of a brain transduced with AAV-PHP.eB:NSE-H2B-mCherry[56–58] and counterstained by RedDot2 (RD2) for nuclear staining, which is cleared by the CUBIC-L/R+ protocol (Supplementary Fig. 1 and Supplementary Video 1). The two signals were merged at exactly the same position and could thus be analyzed easily (Fig. 3e).

MOVIE advanced high-speed imaging system

When scanning samples in the z direction (depth), conventional microscopes use the of 'stop and exposure' scheme, which is performed with the stage stopping each time after moving to the specified position, and, therefore, total imaging duration is mainly determined by the positioning time because
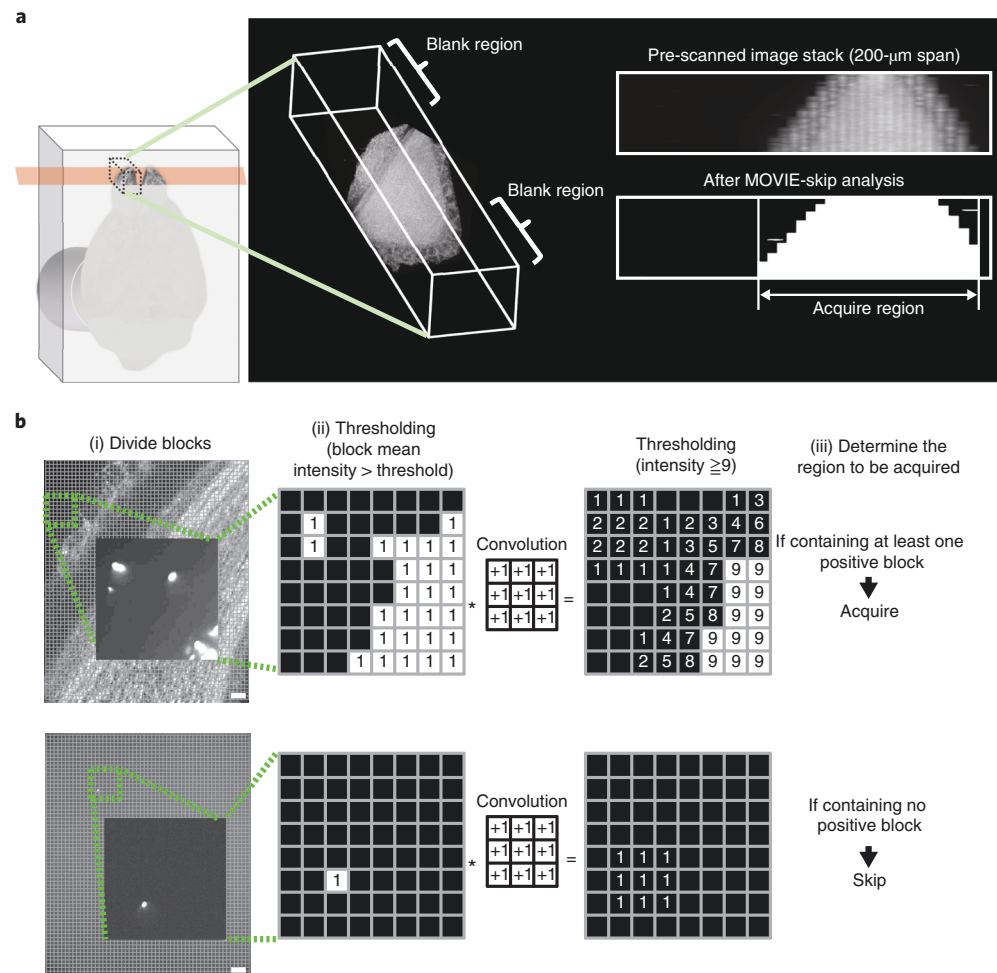
Fig. 6 | Details of MOVIE-skip. a, The olfactory bulb of a PI-stained mouse brain is illustrated; the image contains blank regions. After MOVIE-skip, only the specified region was imaged (i.e., the blank regions were not imaged). **b**, For stable skipping, the block convolution method was developed. Pre-scan was performed at the time of going back to the z-start position of the next stack at a speed of ~200 μm/exposure time. We use the following scheme (i—iii) in order to ignore small particles outside of the sample; two examples are shown in this figure using the zoomed area. (i) Divide an image into some size of blocks (e.g., when the block size of 40 × 40 pixels is chosen, an image whose size is 2,160 × 2,560 pixels will be divided into 3,456 blocks). (ii) Perform threshold binarization, comparing the mean intensity of each block with the threshold. The threshold was typically set to two times the value of the mean intensity of the image in the blank region. In this figure, positive blocks were painted white. (iii) Convolve the image with the described square 3 × 3 kernel, and perform threshold binarization with nine. With at least one positive block, the image is acquired; otherwise the image is skipped. Scale bars, 100 μm.

Table 1 | Nuclear stain stability in CUBIC reagents

	CUBIC-R+	CUBIC-X2
Propidium iodide	Stable	Stable
RedDot2	Stable	Untested
SYTO 16	Unstable	Untested

the positioning takes much longer than the actual exposure time (e.g., 150 ms of stage motion between exposures in our previous work)[11] (Fig. 4a). Figure 4b shows the imaging speed at various stage-positioning times. The stage-positioning time depends on the motor type and accuracy of the position. When using a typical stepping-motor-type stage, the positioning time is estimated to be ~100–150 ms. Therefore, in the case of a short exposure time, the imaging time is mainly determined

by the stage-positioning time. Stage acceleration and deceleration are time consuming and may cause the image to blur. When using a piezo-type stage, the stage-positioning time can be shortened, but, in our experience, it is ~30–50 ms. To overcome this limit, we developed the MOVIE-scan method. With MOVIE-scan, the combination of uniform motion of the stage with synchronized continuous acquisition can reduce the overall imaging time (Fig. 4a). The relationship between exposure time and the imaging throughput is shown in Fig. 4b. The apparent sheet thickness depends on the stage-moving distance in an acquisition cycle (Fig. 4c). Typically when using MOVIE, we set the acquisition cycle time of an image to 55 ms, the moving distance to 5 μm and the z-stage speed to 5 μm/55 ms (i.e., 90.9 μm/s). Although the apparent sheet thickness corresponds to 8.95 μm, evaluated by the FWHM of the axial direction (Fig. 4c), compared with 7.80 μm without MOVIE (in a 'stop and exposure' mode using the same stage), the imaging throughput became 18.2 frames per s (fps) (Fig. 4b, 1/exposure time is 20), compared with 4.4 fps without MOVIE.

The required imaging time can be shortened by MOVIE-scan. However, when using MOVIE-scan (and also a 'stop and exposure' mode), an additional issue is that the focal plane can shift for various reasons. Some samples may be less transparent at deeper areas because of limitations of the tissue-clearing method, storage duration and fixation condition of samples. It is also difficult to match the RIs of the sample, embedded gel, and immersion oil completely. Therefore, efficient autofocusing techniques have been developed[59–63]. Typically, autofocus must be performed frequently to collect images that are in focus throughout. Conventional autofocus systems need extra tens of images to determine the optimal focus with stage stopping (we refer to this as 'stop and exposure' autofocus), and this scheme is commonly used for autofocusing. In the MOVIE system, an efficient real-time autofocus mode (MOVIE-focus) is used to adjust light-sheet positions without acquisition of any extra images. (Fig. 5) The image quality can be evaluated by various image quality metrics. We chose Shannon entropy of the normalized discrete cosine transformation (DCTS) for image quality metric calculations, as this was suggested as the best method in a previous report[60]. Next, we simulated the autofocus method by using datasets from a propidium iodide (PI)-stained mouse brain with 400,000 images, which were acquired at 0- to 5,000-μm depth every 5 μm with 400 different light-sheet positions at 0.35-μm intervals. The frequency of autofocus was mainly influenced by the number of images required for determining the next light-sheet position, and the time for calculating the image quality metric for each image. In MOVIE-focus, we continuously generate and evaluate two slightly different light-sheet positions by calculating the image quality metrics of two images before and after the change of the light-sheet position, and the 'focus value' is calculated at each light-sheet position (Fig. 5b). Once the 'focus value' crosses the threshold (in this paper, we used 3 or −3), the center of the light-sheet oscillation is updated (Fig. 5c). After updating a light-sheet position, the 'focus value' is initialized to 0 and the autofocus sequence is repeated. In this protocol, the 'focus value' calculation is performed for each exposure, but MOVIE-focus can also work if used for every second or third exposure. If the frequency is set to be low, the tracking ability will be poor and may cause defocusing with non-uniform samples. To achieve real-time processing in high-speed imaging, the processing time is decreased to <10 ms per image by dividing the images into blocks and selecting the blocks with high L^2-norm values. Typically, we divide a 2,160 × 2,560-pixel image into 128 × 128-pixel blocks, resulting in 320 blocks, and selected the top 32 blocks (top 9.5% of the image size) by L^2-norm. Then DCTS of each selected block is calculated and the DCTS score is given by taking the summation of all selected blocks. Last, the DCTS scores of two images are compared, and the image with higher DCTS score is chosen as the better focus direction, and the 'focus value' is updated by +1 or −1, corresponding to better focus direction. The details of the various parameters are explained in Supplementary Fig. 2. Typical results of autofocus simulation, ideal focus positions, MOVIE-focus and stop-and-exposure autofocus at each 100–1,000 μm are shown in Fig. 4d. The distances from ideal light-sheet positions are shown in Fig. 4e. In MOVIE-focus, >97% of light-sheet positions were within 3 μm of the ideal focus positions. The mean distance from ideal focus positions was 1.15 μm, corresponding approximately to stop-and-exposure autofocus every 250 μm. Figure 4f illustrates the tracks of MOVIE-focus on the landscape of the relation among light-sheet position, depth and relative DCTS value. As shown in Fig. 4f, MOVIE-focus keeps the fine light-sheet position throughout; the images are shown in Supplementary Figs. 3,4 and Supplementary Video 2. Typically, we use the nuclear staining channel for MOVIE-focus, because the signal is usually high and distributed throughout the sample. In addition, when applying a fluorescent protein or immunostaining channel to MOVIE-focus, it performs well with the same focusing parameters, as long as the signal is present in all imaging areas to allow the evaluation of the image quality metric.
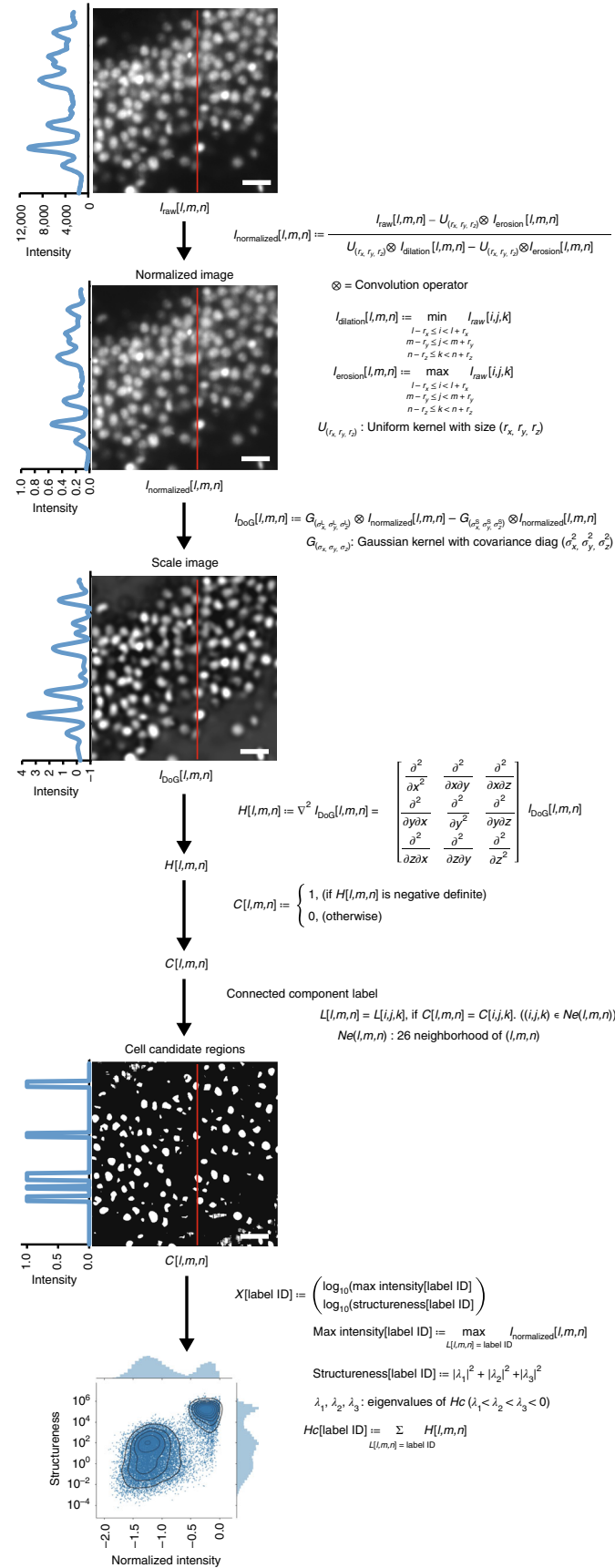
The blank regions outside the sample are usually imaged because of the entire coverage of the whole organ, and plenty of extra images are acquired, extending total imaging time and downstream data analysis time. In the MOVIE system, to shorten imaging time by skipping blank regions, the z-start and z-end positions are specified at each stack by the evaluation of whether the intensity of the pre-scanned images is beyond the specified threshold. Pre-scan is performed during the time in which the scan goes back to the z-start position of the next stack at the speed of up to 200 μm per acquisition cycle time. The total data amount for a whole mouse brain was reduced by >50% by using MOVIE-skip (Figs. 4g,6 and Supplementary Video 3).
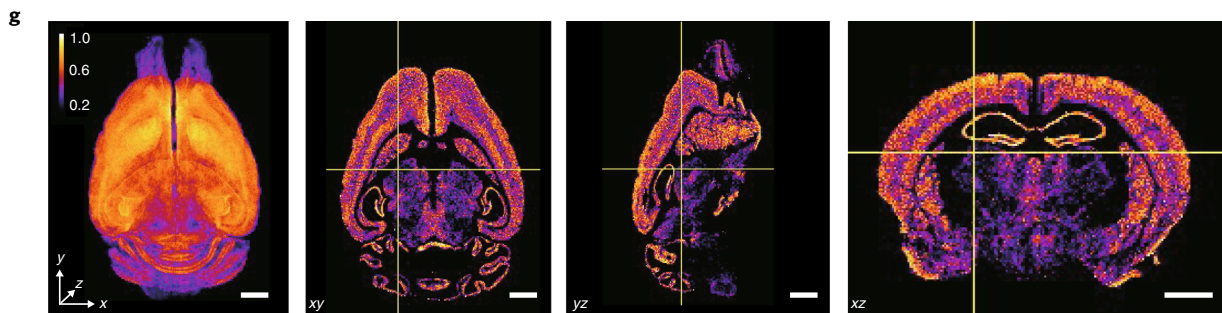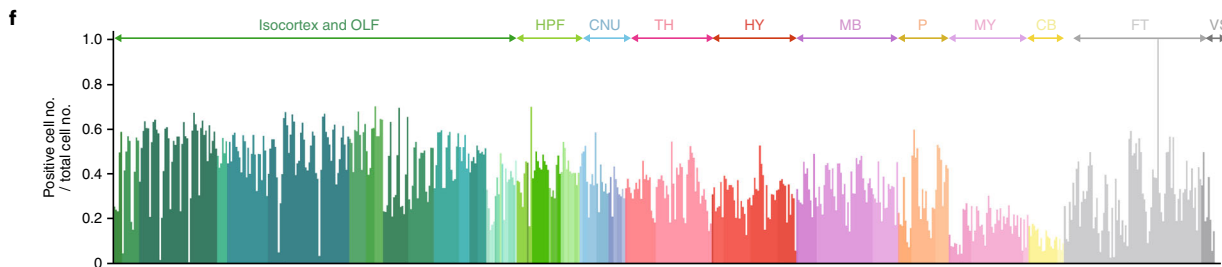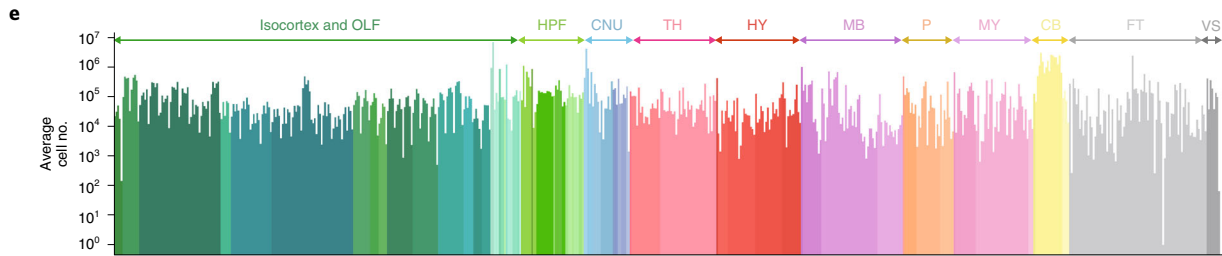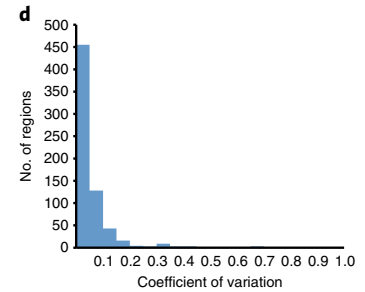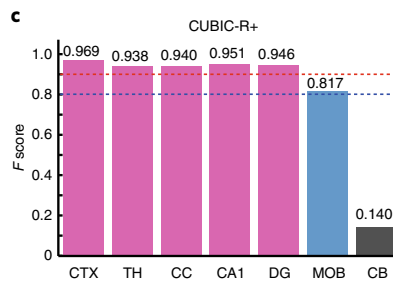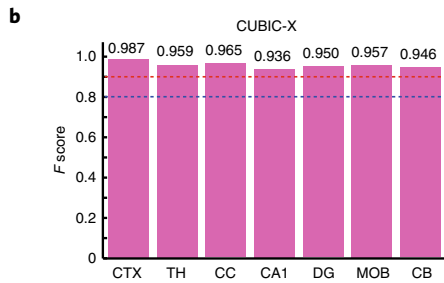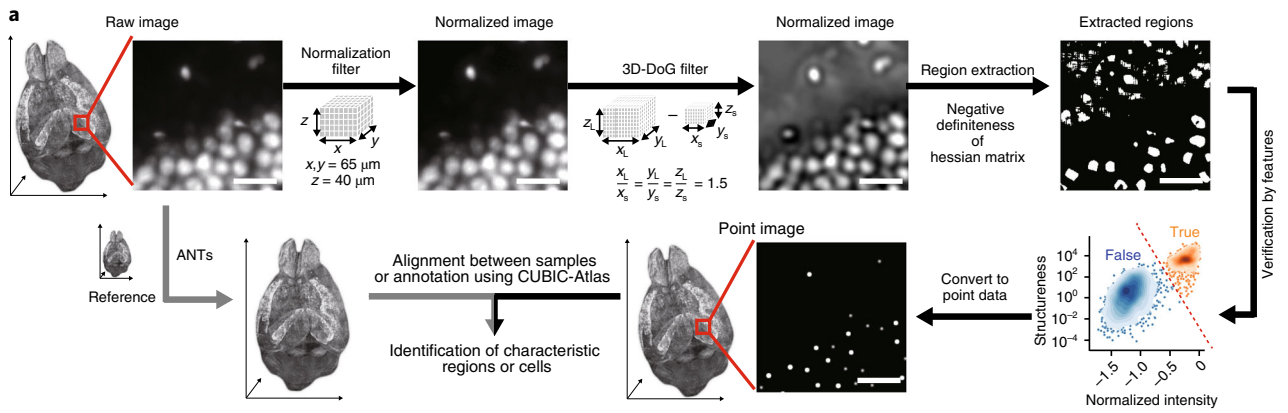
Cell-nucleus detection and annotation

The HDoG_gpu.py script, followed by the MergeBrain.py and HDoG_classifier.py scripts, which will be obtained in Step 13 ('Software setup'), is used to attempt to detect all cells in raw images (Figs. 7,8a). The first step of cell-nucleus detection is normalization of the signal intensity because the illumination light-sheet intensity at deep areas in a sample is decreased by light absorption of dyes or other light-absorbing substances. The normalized images are processed by a 3D difference-of-Gaussian (DoG) filter, which is a band-pass filter defined as the difference between two sizes of Gaussian-filtered images. This filter discards spatial information smaller or larger than the two-filter size while preserving information in the scale between the two sizes. Although the theoretical foundation of this scale selection by Laplacian of Gaussian (LoG) filtering was pioneered by Lindeberg[64], DoG is more suitable to processing on GPUs. After scale selection by the 3D-DoG filter, the convexity of intensity variation at each voxel, which is the negative definiteness of the Hessian matrix, is verified. If a voxel is judged to be convex, it is considered to be part of a cell nucleus. If the neighboring voxels are also convex, these connected voxels are labeled with the same ID number and considered to be a cell-nucleus candidate. Fast implementations of connected component labeling for GPUs have been considered previously[65,66]. For each region, maximum intensity in the region of the normalized image and structureness index are calculated as features of that region and manually classified into two clusters. A cluster with higher intensity and higher structureness corresponds to the cluster of cell nuclei (Figs. 7,8a). Structureness index is defined by using eigenvalues of the Hessian matrix, a principle first proposed by Frangi et al.[67]. After the identification of true cell nuclei by features, the centroid coordinates of identified regions are transformed to the whole-organ coordinate system (Fig. 8a). The accuracy of the cell-nucleus-detection program was evaluated by comparison with manual detection. An adult mouse brain cleared with the CUBIC-X protocol showed >90% accuracy over all the brain and the CUBIC-R+-treated brain showed >90% accuracy, except for the areas with extremely high cell densities such as the olfactory bulb (main olfactory bulb (MOB), 14%) and cerebellum (CB, 82%) (Fig. 8b,c).

For comparative analysis, cell coordinates are further transformed to a standard coordinate system, which is defined by a reference organ. Even when a standard reference is not available, an arbitrary selection from among the samples is enough to be a reference for inter-sample comparison. Transformation parameters are calculated by ANTs software[68] with downscaled images. When users analyze the mouse brain, the AtlasMapping.py script can be used for alignment and annotation of the anatomical region information.

Fig. 7 | Details of cell-nucleus-detection algorithm. First, raw images (I_{raw}) are normalized ($I_{normalized}$) considering ▶ local amplitude of intensity variation. If the intensity of a voxel is the local minimum, which roughly corresponds to the tail of the cells or an empty region, its normalized intensity is defined as 0. On the other hand, if the voxel is the local maximum, which corresponds to the center of a cell, normalized intensity is defined as 1. As the simple local maximum ($I_{dilation}$) or local minimum ($I_{erosion}$) images are sensitive to small noises in intensity, they are smoothed by a uniform filter $U_{(rx,ry,rz)}$. Next, normalized images undergo scale selection by DoG filter. The DoG filter is defined as the difference between the larger Gaussian $G_{(\sigma_x^L,\sigma_y^L,\sigma_z^L)}$ filtered image and the smaller Gaussian $G_{(\sigma_x^S,\sigma_y^S,\sigma_z^S)}$ filtered image. Each voxel in DoG-filtered images is checked for whether the Hessian matrix is negative definite or not. If the intensity profile is convex upward at the voxel, the Hessian matrix at the voxel is negative definite and $C[l,m,n]$ is 1. Otherwise, $C[l,m,n]$ is 0. Next, connected component analysis is performed and each connected region is labeled with a unique ID, and these are defined as cell candidate regions. Finally, the candidates are verified by their features. Max intensity is defined as maximum normalized intensity in the region, whereas structuredness of the region is defined as the sum of squared eigenvalues of the Hessian matrix of that region. Note that the Hessian matrix of a region is defined as the sum of the Hessian matrix of all voxel components. This 2D feature vector represents how much each candidate region resembles a cell. As it is plotted in the figure, true cells (top-right cluster) and noisy candidates (bottom-left cluster) show clear separation. Scale bars, 50 μm.

$I_{raw}[l,m,n]$

$$I_{normalized}[l,m,n] := \frac{I_{raw}[l,m,n] - U_{(r_x, r_y, r_z)} \otimes I_{erosion}[l,m,n]}{U_{(r_x, r_y, r_z)} \otimes I_{dilation}[l,m,n] - U_{(r_x, r_y, r_z)} \otimes I_{erosion}[l,m,n]}$$

Normalized image

$\otimes$ = Convolution operator

$$I_{dilation}[l,m,n] := \min_{\substack{l - r_x \leq i < l + r_x \\ m - r_y \leq j < m + r_y \\ n - r_z \leq k < n + r_z}} I_{raw}[i,j,k]$$

$$I_{erosion}[l,m,n] := \max_{\substack{l - r_x \leq i < l + r_x \\ m - r_y \leq j < m + r_y \\ n - r_z \leq k < n + r_z}} I_{raw}[i,j,k]$$

$U_{(r_x, r_y, r_z)}$: Uniform kernel with size (r_x, r_y, r_z)

$I_{normalized}[l,m,n]$

$$I_{DoG}[l,m,n] := G_{(\sigma_x^1, \sigma_y^1, \sigma_z^1)} \otimes I_{normalized}[l,m,n] - G_{(\sigma_x^0, \sigma_y^0, \sigma_z^0)} \otimes I_{normalized}[l,m,n]$$

$G_{(\sigma_x, \sigma_y, \sigma_z)}$: Gaussian kernel with covariance diag $(\sigma_x^2, \sigma_y^2, \sigma_z^2)$

Scale image

$I_{DoG}[l,m,n]$

$$H[l,m,n] := \nabla^2 I_{DoG}[l,m,n] = \begin{bmatrix} \frac{\partial^2}{\partial x^2} & \frac{\partial^2}{\partial x \partial y} & \frac{\partial^2}{\partial x \partial z} \\ \frac{\partial^2}{\partial y \partial x} & \frac{\partial^2}{\partial y^2} & \frac{\partial^2}{\partial y \partial z} \\ \frac{\partial^2}{\partial z \partial x} & \frac{\partial^2}{\partial z \partial y} & \frac{\partial^2}{\partial z^2} \end{bmatrix} I_{DoG}[l,m,n]$$

$H[l,m,n]$

$$C[l,m,n] := \begin{cases} 1, & \text{(if } H[l,m,n] \text{ is negative definite)} \\ 0, & \text{(otherwise)} \end{cases}$$

$C[l,m,n]$

Connected component label

$L[l,m,n] = L[i,j,k]$, if $C[l,m,n] = C[i,j,k]$. $((i,j,k) \in Ne(l,m,n))$

$Ne(l,m,n)$: 26 neighborhood of (l,m,n)

Cell candidate regions

$C[l,m,n]$

$$X[\text{label ID}] := \begin{pmatrix} \log_{10}(\text{max intensity[label ID]}) \\ \log_{10}(\text{structureness[label ID]}) \end{pmatrix}$$

$$\text{Max intensity[label ID]} := \max_{L[l,m,n] = \text{label ID}} I_{normalized}[l,m,n]$$

$$\text{Structureness[label ID]} := |\lambda_1|^2 + |\lambda_2|^2 + |\lambda_3|^2$$

$\lambda_1, \lambda_2, \lambda_3$: eigenvalues of Hc $(\lambda_1 < \lambda_2 < \lambda_3 < 0)$

$$Hc[\text{label ID}] := \sum_{L[l,m,n] = \text{label ID}} H[l,m,n]$$

Using this cell-nucleus-detection algorithm, we re-counted the cells in the 8-week-old C57BL/6J mouse brain from which data had been obtained when preparing the CUBIC-Atlas in our previous report[11]. As a result, we observed 1.03×10^8 cells, and the CUBIC-Atlas was updated using this result

◀ **Fig. 8 | Cell-nucleus detection and alignment. a**, Scheme of cell-nucleus detection and alignment between samples and reference organ. Scale bars, 50 μm. **b**, Validation of cell-nucleus-detection accuracy at each anatomical region of a CUBIC-X-treated brain. **c**, Validation of cell-nucleus-detection accuracy at each anatomical region of a CUBIC-L/R +-treated brain. **d**, A histogram of coefficient of variation for each anatomical region. **e**, Average cell number of all anatomical regions in three 8-week-old C57BL/6N mouse brains. Only the edge regions (i.e., having no child region) are shown. **f**, Positive cell number ratio of each anatomical region in AAV-PHP.eB (NSE-H2B-mCherry)-infected mouse brain. **g**, 3D and cross-section images of the positive cell number ratio map of AAV-PHP.eB (NSE-H2B-mCherry)-infected whole mouse brain. Voxel size, 80 μm. Scale bars, 2 mm. CA1, field CA1; CB, cerebellum; CC, corpus callosum; CNU, cerebral nuclei; CTX, cerebral cortex; DG, dentate gyrus; FT, fiber tract; HPF, hippocampal formation; HY, hypothalamus; MB, midbrain; MOB, main olfactory bulb; MY, medulla; OLF, olfactory areas; P, pons; TH, thalamus; VS, ventricular system. All experiments followed the relevant governmental and institutional guidelines for animal experiments.

(termed v.1.2). Next, we also reanalyzed the cell number of the whole brain and each anatomical region of three 8-week-old mice (C57BL/6N) that were cleared with CUBIC-X protocol (Fig. 8e). As a result, the average total cell number was found to be 9.77 ($\pm$0.46) $\times$ 10^7, in contrast to 7.22 ($\pm$0.52) $\times$ 10^7 in our previous report[11]. The coefficient of variation (CV) was 4.75% for whole brain, and 67.8% of the regions (455/671 regions) showed <5% CV. (Fig. 8d). We next quantified the whole-brain infection efficiency of AAV-PHP.eB (NSE-H2B-mCherry). We used the signal intensity ratio of the first channel (nuclei stain) to the second channel (mCherry) to determine which cells were positive, because intensity of the excitation laser was decreased in the deep areas and signal intensity detected through an objective lens was also decreased, requiring correction. The ratio of mCherry$^+$ cells in each anatomical region was quantified by using CUBIC-Atlas (Fig. 8f). In addition, we visualized the localization of mCherry$^+$ cells by using the mCherry$^+$ cell number ratio in each 80-μm voxel (Fig. 8g). These results show that the cortex and hippocampus, corresponding to the pyramidal layer of Ammon's horn (CAsp) and the granule cell layer of the dentate gyrus (DG-sg), respectively, showed higher positive ratios than other areas. These analysis programs confirmed that the expanded CUBIC-X-treated mouse brain could be analyzed within 8 h (14 TB) and CUBIC-L/R+-treated brains could be analyzed within 2 h (2.5 TB) using our analysis server with 28 dual-CPU cores and four GPUs.

Expertise needed to implement the protocol

The procedures described here require some prior experience in sampling organs, building light-sheet microscopes and programming or software development. The most effective and time-efficient implementation of these protocols is achieved when anatomical knowledge and skills in organ sampling are available, as well as knowledge and familiarity with Python for cell-nucleus detection, annotation and comparison of different samples with CUBIC-Atlas or ANTs software. If a commercially available microscope is not available, an optical engineer who has experience in building optical instruments and controlling electronics for hardware and automation is required.

Limitations of the current CUBIC pipeline

CUBIC reagents and procedures have been improved to facilitate preparation of highly transparent whole-organ and whole-body samples and have been applied to various research fields, including neuroscience, cancer research and pathology. Further applications are expected, because our recent report also provided clearing methods for bone and human organ blocks[10]. Other groups have also improved CUBIC and applied it to various organisms such as fly (FlyClear)[69], crustaceans[70] and plants (ClearSee)[71]. Transparency of whole mouse organs with the current CUBIC protocol is sufficient for high-resolution imaging and it is also compatible with fluorescent protein and immunostaining. However, the current CUBIC reagents are not capable of clearing some pigments, such as melanin and lipofuscin, completely. In addition, the lipid removal from large specimens such as rat, marmoset and human are still inefficient. Therefore, improvements in the transparency and processing time of whole-organ or whole-body clearing of larger organisms are required. Regarding volumetric imaging, we showed that it is possible to markedly increase the volumetric imaging speed with the MOVIE system, but it still has resolution limits due to optical limits, especially those pertaining to z-resolution-related issues with light-sheet generation. Regarding data analysis, there are still challenges for segmentation and detection of the precise morphology of each cell at the whole-organ scale within a practical time. Because the clearing reagents, imaging methods and data analysis algorithms used in the CUBIC pipeline are continually being improved and developed, there is a possibility that these problems will be solved in the near future.

Materials

Biological materials

- Animal samples. We usually use C57BL/6N (CLEA Japan, cat. no. C57BL/6NJcl) or C57BL/6J (Charles River Laboratories, cat. no. C57BL/6J) mice to prepare cleared organs. For virus-infected samples, 8-week-old mice receive intravenous administration of AAV-PHP.eB (NSE-H2B-mCherry, 6.4×10^{11} viral genome) through the retro-orbital sinus as previously described[72]. The perfusion fixation is done at 1 month after viral injection **! CAUTION** Animal experiments must be performed in accordance with governmental and institutional rules. All animal experiments and housing conditions in this report were authorized by the animal care and use committees of the RIKEN Institute, The University of Tokyo and Gunma University, and all animals were treated humanely in accordance with the relevant institutional guidelines for experiments using animals.

Reagents

Perfusion, fixative and storage reagents

- PBS tablets (pH 7.4; Takara, cat. no. T9181)
- Sodium azide (Nacalai Tesque, cat. no. 31208-82) **! CAUTION** Sodium azide is toxic. Avoid its inhalation and contact with the skin or eyes.
- D-PBS (no calcium, no magnesium; Gibco, cat. no. 14190-144)
- Paraformaldehyde phosphate buffer solution (PFA; 4%; Wako, cat. no. 163-20145) **! CAUTION** PFA is toxic. Perform all procedures in a fume hood. Avoid inhalation and exposure to the skin or eyes.
- Sucrose (Nacalai Tesque, cat. no. 30403-55 or 30404-45)
- NaCl (Nacalai Tesque, cat. no. 31320-05 or 31319-45)
- Tissue-Tek OCT compound (Sakura Finetek, cat. no. 4583)
- Ethanol (Japanese Pharmacopoeia, cat. no. 324-00037)
- dH_2O
- Anesthetizing agents (such as pentobarbital (Kyoritsu Seiyaku, cat. no. 21009), ketamine (Daiichi Sankyo, cat. no. 1119400A2038)/xylazine (ZENOAQ, cat. no. 904150) or isoflurane (Pfizer Japan, cat. no. 114133403))

Tissue-clearing and nuclei-staining reagents

- Tissue-clearing reagent CUBIC-L (for animals; Tokyo Chemical Industry, cat. no. T3740) **▲ CRITICAL** CUBIC-L can be prepared as described in the 'Reagent setup' section, but pre-mixed and quality-controlled solution is also commercially available.
- Tissue-clearing reagent CUBIC-R+ (for animals; Tokyo Chemical Industry, cat. no. T3741) **▲ CRITICAL** Tissue-clearing reagent CUBIC-R+ (for animals) can alternatively be prepared as described in the 'Reagent setup' section.
- *N*-Butyldiethanolamine (Tokyo Chemical Industry, cat. no. B0725)
- PEG mono-*p*-isooctylphenyl ether (Triton X-100; Nacalai Tesque, cat. no. 12967-45)
- 2,3-dimethyl-1-phenyl-5-pyrazolone (antipyrine; Tokyo Chemical Industry, cat. no. D1876)
- Nicotinamide for CUBIC-R+(nicotinamide (N)) (Tokyo Chemical Industry, cat. no. N0078)
- *N*-Methylnicotinamide for CUBIC-R+(*N*-methylnicotinamide (M)) (Tokyo Chemical Industry, cat. no. M0374)
- *N*,*N*,*N*′,*N*′-Tetrakis(2-hydroxypropyl)ethylenediamine (Quadrol; Tokyo Chemical Industry, cat. no. T0781)
- Urea (Nacalai Tesque, cat. no. 35904-45 or 35907-15)
- Imidazole (Tokyo Chemical Industry, cat. no. I0001)
- Propidium iodide (PI; Life Technologies, cat. no. P21493) **! CAUTION** PI is light sensitive.
- RedDot2 (RD2; Biotium, cat. no. 40061) **! CAUTION** RD2 is light sensitive.

Imaging reagents

- Agarose for CUBIC-R+ (Nacalai Tesque, cat. no. 01163-76) **▲ CRITICAL** Gelation properties of agarose vary depending on the producer. To fully reproduce our results, use appropriate agarose from listed vendors. If the combination of CUBIC and agarose is not suitable, it will not gel or become transparent. If recommended agaroses are not available, high-melting-point or high-strength agaroses may be alternatives.
- Agarose S for CUBIC-X2 (Nippon Gene, cat. no. 318-01195) **▲ CRITICAL** The same cautions as above apply to the appropriate choice of gelatin.
- Mineral oil (Sigma-Aldrich, cat. no. M8410)

- HIVAC F-4 (Shin-Etsu Chemical, cat. no. HIVAC-F4)
- Sphero fluorescent particles (purple; 0.1–0.3 μm, 1.0% (wt/vol); Spherotech, cat. no. FP-0262-2)

Equipment
Tissue clearing
- Tubes (5 ml; Eppendorf, cat. no. 0030 119.401)
- Conical tubes (15 ml; Corning, cat. no. 352096 or Greiner, cat. no. 188271)
- Conical tubes (50 ml; Corning, cat. no. 352070 or Greiner, cat. no. 227261)
- Intravenous injection needle (23 gauge; butterfly type; Terumo, cat. no. SV-23CLK)
- Injection needle (26 gauge × 1/2-inch; Terumo, cat. no. NN-2613S)
- T-shape stopcock (Terumo, cat. no. TS-TL2K)
- Disposable syringes (10 or 20 ml; Terumo, cat. no. SS-1010SZ or SS-20ESZ)
- Incubation devices. We use a hybridization incubator (Taitec, model no. HB-80) or incubator (Eyela, model no. FMS-1000 or MHS-2000)
- Shaker (Taitec, model no. Wave-PR or MixerXR-36)
- Magnetic stirrer (Ikeda Scientific, cat. no. IS-20P)
- Hot stirrer (Advantec, cat. no. SRS710HA)
- Water bath (Advantec, cat. no. TBX183SB)
- Abbe refractometer (Atago, cat. no. DR-A1)
- pH meter (Horiba Scientific, LAQUAtwin model)
- Microwave oven (National, cat. no. NE-S12)
- Fume hood (Shimadzu, cat. no. CBR-Rc)
- Gel embedding mold
- Acrylic plates with polished edges (Hazaiya, 50 mm × 14 mm × 6 mm (2×), 45 mm × 14 mm × 6 mm (2×), 75 mm × 56 mm × 6 mm (2×))

Customized LSFM and operation computer
- Optical table with tapped holes (Herz, model no. h-TDIS-3012LA M6-25XY tap)
- SOLE- Laser Light Engine (Omicron Laserage, model no. SOLE-3)
- Optical posts (Thorlabs, part nos. TR50/M (24×),TR150/M (8×), RS5/M (4×), RS4P/M (4×), RS25/M (4×))
- Post holders (Thorlabs, part nos. PH50/M (24×) and PH100/M (8×))
- Base adaptor (Thorlabs, part nos. BE1/M (6×) and CF125/M (6×))
- ER assembly rods (Thorlabs, part nos. ER1.5 (16×), ER2 (40×) and ER4 (48×))
- Lens mounts (cage plates; Thorlabs, part nos. CP03/M (16×), CP02T/M (2×), CP02B (4×), CXYZ05/M (2×), CXY1 (14×))
- Achromatic doublet lenses (Thorlabs, part nos. AC127-030-A-ML, AC127-050-A (2×), AC254-050-A (6×), AC254-100-A (4×) and AC254-150-A-ML)
- Iris (Thorlabs, part no. CP20S (2×))
- Motorized filter flip mounts (Thorlabs, part no. MFF101/M) for laser switching
- Broadband dielectric mirrors (Thorlabs, part no. BB1-E02 (4×))
- Kinematic mirror mounts (Thorlabs, part no. KM100CP/M (3×))
- Galvano mirrors (Thorlabs, item nos. GVS001/M (6×), GCE001 (6×), GCM001 (6×), B1C/M (6×) and GHS003/M (6×))
- Galvo system linear power supply (Thorlabs, model no. GPS011 (3×))
- Objective lenses for excitation (CFI Plan Achromat 4×; Nikon, part no. MRL00042 (2×))
- Detection objective lens (Olympus, model no. XLPLN10XSVMP)
- Lens adaptors (Thorlabs, item nos. SM1A12 (2×), SM1L10 (2×))
- Customized sample chamber (inner size: width (W) 80 mm × depth (D) 60 mm × height (H) 120 mm or W 80 mm × D 60 mm × H 160 mm, acrylic plastic; ISAX)
- Customized sample holder (inner size: W 35 mm × D 15 mm × H 14 mm; ISAX)
- Breadboard (OptoSigma, model no. OBC-2030 25XY-M4 tap)
- Precise lab jack (OptoSigma, model no. LJA-16223)
- xy stages (Thorlabs, part nos. MTS50-Z8E (2×) and MTS50C-Z8)
- z stage (Autex, part no. RTP-2035/00100)
- θ stage (Physik Instrumente, part no. M-116.DG)
- Emission filter (2-inch; Chroma Technology, part no. ET625/30m)
- Emission filter (1-inch; Thorlabs, part no. FB700-40)

- Fixed mirror mounts (2-inch; Thorlabs, part no. FMP2/M)
- SM1 lens tube (Thorlabs, part no. SM1L03)
- Adaptor with external C-mount (Thorlabs, part no. SM1A9)
- Dichroic mirror (Thorlabs, part no. DMSP650L)
- Detection tube lenses (Thorlabs, part no. AC508-180-A-ML (2×))
- Two-axis miniature dovetail translation stages (Thorlabs, part no. DT12XY/M)
- Post-mountable *xy* translation mounts (Thorlabs, part no. LM2XY (2×))
- sCMOS cameras (Andor, model no. Zyla 5.5 (2×))
- Medium metric low-profile optical rail (800 mm; OptoSigma, part no. OBT-800SH)
- Large metric low-profile optical rail (500 mm; OptoSigma, part no. OBT-500LH)
- Medium metric optical carrier (60 mm; OptoSigma, part no. CAA-60LS (4×))
- Large metric optical carrier (120 mm; OptoSigma, part no. CAA-120L (3×))
- Virtual bench (National Instruments, model no. VB-8012)
- Compact data acquisition (DAQ) devices (National Instruments, model nos. NI cDAQ-9171 and NI cDAQ-9174)
- Analog output module (National Instruments, model nos. NI9263 (4×))

Computer
- PC (Unitcom, model no. Sol-TT9W-Xe5D-GXS; Windows 10 Pro, 64 bit; CPU: dual Intel Xeon E5-2630V4; memory: DDR4-2400 ECC Reg, 8 GB (16×); GPU: GeForce, model no. GTX 1080, Serial-ATA SSD (solid-state drive) (240 GB))
- Computer server (analysis server; Japan Computing Systems, model no. VC82690v4-4UXQTA2-GPK; data storage server, JBOD)
- InfiniBand card (Mellanox, product no. MCX353A-FCBT FDR PCIe3.0) for microscope operation PC
- InfiniBand card (Mellanox, product no. MCX354A-FCBT, FDR PCIe3.0) for data server
- InfiniCable (Mellanox, product no. MC220731V-010, 56 GB/s, QSFP, 10m)
- InfiniBand Switch system (Mellanox, product no. MSX6012F-1BFS)
- CPUs (Intel, Xeon E5-2690v4, 2.60 GHz 14C/28T (2×))
- GPUs (NVIDIA, GeForce GTX1080Ti, 11 GB (4×))
- Memory (DDR4 2400 ECC, registered 16 GB (16×))
- SSD (Intel, S4500 1.92 TB (5×), RAID 0)
- Raid card (Broadcom, cat. no. LSI 3108)
- Case (4U rackmount; Japan Computing Systems, cat. no. VCXQTA2-GPKT)
- Operating system (CentOS 7.5, https://www.centos.org/download/)
- Uninterruptible power supply (APC, Smart-UPS XL 3000 RM 200V)
- Chassis (4U rackmount; Japan Computing Systems, cat. no. HDD 44 Bay JBOD (2×))
- Hard drive (HDD; SATA, 8TB, 7,200 r.p.m. (60×), RAID 60)

Software and tools
- ImageJ (free-software from the US National Institutes of Health (NIH), https://imagej.nih.gov/ij/)
- Imaris (Bitplane, http://www.bitplane.com/imaris/imaris) for visualization of 3D images
- Python v,3.6 (https://www.python.org/downloads/)
- GNU Compiler Collection 4.8 for compiling C++11 (https://gcc.gnu.org/releases.html)
- CMake 2.8 (https://cmake.org/download/)
- CUDA Toolkit 9.0 (https://developer.nvidia.com/cuda-90-download-archive)
- Visual Studio C# for MOVIE system (https://visualstudio.microsoft.com/downloads)
- 64-bit LabVIEW for LSFM control (https://www.ni.com/en-us/support/downloads/software-products/download.labview.html#305933)
- ANTs 2.1.0 (freeware from stnava: https://github.com/ANTsX/ANTs/releases)
- CUBIC-Atlas v.1.2 (http://cubic-atlas.riken.jp)

Reagent setup
CUBIC-L
CUBIC-L is a mixture of 10% (wt/wt) *N*-butyldiethanolamine and 10% (wt/wt) Triton X-100 in dH$_2$O. For example, to prepare 100 g of CUBIC-L solution, mix 10 g of *N*-butyldiethanolamine and 10 g of Triton X-100 in 80 g of dH$_2$O with a stirrer at room temperature (22–26 °C). The reagent can be stored at room temperature for up to 6 months. CUBIC-L can alternatively be purchased (Reagents).

Half-diluted CUBIC-L

Half-diluted CUBIC-L is an equivalent-volume mixture of CUBIC-L and dH_2O. Half-diluted CUBIC-L can be stored at room temperature for up to 6 months.

CUBIC-R+(N)

CUBIC-R+(N) is a mixture of 45% (wt/wt) antipyrine, 30% (wt/wt) nicotinamide, 0.5% (vol/vol) N-butyldiethanolamine and dH_2O. To prepare 100 g of CUBIC-R+ solution, dissolve 45 g of antipyrine and 30 g of nicotinamide in 25 g of dH_2O. After complete dissolution, add 250 µl of N-butyldiethanolamine to 50 ml of the mixture so that the pH becomes 9.6–9.8 and the RI is 1.522 (see 'Troubleshooting' section). CUBIC-R+(N) can be stored at room temperature for up to 6 months.

CUBIC-R+(M)

CUBIC-R+(M) is the same formula as that for CUBIC-R+(N), except that it contains N-methylnicotinamide in place of the nicotinamide. CUBIC-R+(M) can alternatively be purchased (Reagents). ▲ CRITICAL The N-methylnicotinamide in CUBIC-R+(M) retains fluorescent protein signals better than nicotinamide. When observing tissues labeled with fluorescent proteins, use CUBIC-R+(M); otherwise, CUBIC-R+(N) can be used, which is inexpensive.

Half-diluted CUBIC-R+

Half-diluted CUBIC-R+ is an equivalent volume mixture of CUBIC-R+ (50% (vol/vol) final concentration) and dH_2O (50% (vol/vol) final concentration). Half-diluted CUBIC-R+ can be stored at room temperature for up to 6 months.

ScaleCUBIC-1

Sca*le*CUBIC-1 is a mixture of 25% (wt/wt) Quadrol, 25% (wt/wt) urea and 15% (wt/wt) Triton X-100. For example, to prepare 100 g of Sca*le*CUBIC-1 solution, dissolve 25 g of urea and 25 g of Quadrol in 35 g of dH_2O with a hot stirrer. After complete dissolution, cool to room temperature and add 15 g of Triton X-100. Sca*le*CUBIC-1 solution can be stored at room temperature for up to 1 month.

Modified-ScaleCUBIC-1

Modified-Sca*le*CUBIC-1 is a mixture of 5% (wt/wt) Quadrol, 25% (wt/wt) urea and 10% (wt/wt) Triton X-100. For example, to prepare 100 g of modified-Sca*le*CUBIC-1 solution, dissolve 25 g of urea and 5 g of Quadrol in 60 g of dH_2O, using a hot stirrer to stop the temperature of the solution from decreasing too much, because this slows dissolution. After complete dissolution, cool to room temperature and add 10 g of Triton X-100. Modified-Sca*le*CUBIC-1 can be stored at room temperature for up to 1 month.

CUBIC-X1

CUBIC-X1 is a mixture of 20% (wt/vol) imidazole and dH_2O. For example, to prepare 100 ml of CUBIC -X1, dissolve 20 g of imidazole in dH_2O at room temperature. CUBIC-X1 can be stored at room temperature for up to 6 months.

CUBIC-X2

CUBIC-X2 is a mixture of 5% (wt/vol) imidazole and 55% (wt/vol) antipyrine in dH_2O. For example, to prepare 100 ml of CUBIC-X2, dissolve 5 g of imidazole and 55 g of antipyrine in dH_2O at room temperature (see 'Troubleshooting' section). CUBIC-X2 can be stored at room temperature for up to 6 months.

Staining buffer

Staining buffer is 1.5 M NaCl in PBS. Staining buffer can be stored at room temperature for up to 1 month.

Immersion oil

For use with CUBIC-R+, mix an ~3:2 ratio of HIVAC F-4 (RI = 1.555) and mineral oil (RI = 1.467) completely with a stirrer. The resulting RI should be 1.522, identical to that of CUBIC-R+, and the mixture ratio should be finely adjusted by monitoring the actual RI. Mineral oil (RI = 1.467) is used for CUBIC-X2. These oils can be used repeatedly for imaging by filtering and clearing contaminants (e.g., clearing reagents, dusts). These oils can be used at room temperature.

Equipment setup

Gel embedding mold

The design of the gel embedding mold is shown in Fig. 2h. The top plate and bottom plate can be replaced with glass slides. For a mouse brain, we use a gel mold with an inner size of 32 mm × 50 mm × 14 mm (the volume is 22.4 ml). ▲CRITICAL The thickness of a gel mold depends on the WD of the objective lens as well as the sample size. ▲CRITICAL The flatness and any scratches on the gel embedding mold plates' surfaces define the gel surface quality and have an effect on image quality. The gel embedding mold must be firmly wiped out with 70% (vol/vol) ethanol or water with a lint-free tissue between uses. ▲CRITICAL The squareness of the gel embedding mold defines the gel's squareness. If the gel squareness is incorrect, the laser light can curve, which has an effect on the optical quality of the samples. When assembling the gel embedding mold, ensure that the gel embedding mold is square.

Customized LSFM for dual-color imaging

We constructed a customized LSFM that was capable of simultaneous dual-color imaging (Fig. 3a). The x-galvanometer mirrors are arranged to generate the illumination light sheet, following the digital-scanned light-sheet microscopy (DSLM) scheme[2]. The y-galvanometer mirrors are arranged to perform the multidirectional selective plane illumination microscopy (mSPIM)[73] to reduce absorption and scattering artifacts. The z-galvanometer mirrors are arranged to control the z-position of the illumination light sheet. Two sCMOS cameras and a dichroic mirror are used for dual-color imaging.

At first, expand and collimate the laser beam with an iris and two achromatic doublet lenses ($f = 30$ and 50 mm). Then place an iris and adjust its diameter to the appropriate size, which corresponds to the illumination sheet thickness (we adjusted to 3 mm, which corresponded to a 7.8-μm illumination sheet thickness). After the iris, switch the laser beam into two paths (right and left excitation) with motorized filter flip mounts. Before the z-galvanometer mirror, shrink the laser beam width with two achromatic doublet lenses ($f = 100$ and 50 mm) because of the limitations of the galvanometer size (5 mm). Place the center of the rotation axis of the z-galvanometer mirror at the front focal points of the before and after achromatic doublet lenses ($f = 50$ mm). Place the center of the rotation axis of the y-galvanometer mirror at the back focal points of the before and after achromatic doublet lenses ($f = 50$ mm). Place the center of the rotation axis of the x-galvanometer mirror at the front focal point of the before and after two achromatic doublet lenses ($f = 50$ mm). After that, collimate the laser beam with an achromatic doublet lens ($f = 100$ mm). Place the illumination objective lenses before an oil chamber. For detection, use an oil immersion detection objective lens with a long (8-mm) WD and high (0.6) NA. Fix the detection objective lens vertically to the side of the custom-made oil chamber. Split the emission signals into two optical paths with a dichroic mirror, then filter and focus the paths onto two sCMOS cameras with achromatic lenses with a 180-mm focal length. Adjust the positions of the achromatic lenses so that the two images merge completely (see 'Troubleshooting' section). Fix the sample to a motorized x–y–z–θ stage through a custom-made sample holder (Fig. 3b). Fill the chamber with an RI-adjusted, appropriate oil (Fig. 3c). We integrate all electronic devices and control them with LabVIEW and a C# program. ▲CRITICAL By using an optical cage system, it is easier to align the optical system. Adjust the position and direction of the lenses and mirrors to pass through the laser beam at the center of an alignment target. We recommend setting the mount screw for the cage rod in the same direction, because a different direction of mount screws causes deformation of the cage system and makes it difficult to adjust the laser beam to the center position.

MOVIE system setup

MOVIE-scan is based on the synchronization of the operation of the z stage as a uniform motion and image acquisition by a sCMOS camera. In addition, MOVIE-focus and MOVIE-skip are necessary for synchronizing galvanometer mirrors (x, y and z) with image analysis. We use digital-to-analog (D/A) converters to synchronize a transistor–transistor logic (TTL) output to the sCMOS camera, laser and galvanometer mirrors. The TTL timing is synchronized with the z stage by LabVIEW, and real-time image analysis of MOVIE-focus and MOVIE-skip is performed by C#. ▲CRITICAL The speed of the z stage must be adjusted, depending on the z-scan range and acquisition cycle time. For example, in this protocol, the z-scan step is adjusted to 5 μm and the acquisition cycle time is 55 ms (exposure time is 50 ms and light-sheet positioning time is 5 ms); thus, the z-stage speed must be set to 91 μm/s (5 μm × 18.2 fps).

High-speed data communication system setup

When using the dual-color MOVIE system, the acquisition rate achieves 36–80 images/s (exposure time, 20–50 ms). Each image is ~11 MB (2,160 × 2,560 pixels, 16 bit), corresponding to 400–890 MB of data/s. We transfer these data directly to an over-storage server with RAID 60 devices, bundling >40 HDDs through a 56-Gbps (gigabits per s) InfiniBand system.

Procedure

Dissection ● Timing 10–15 min

1 Deeply anesthetize the mouse with pentobarbital (~150 mg/kg of body weight) or ketamine (100 mg/kg of body weight)/xylazine (10 mg/kg of body weight) by intraperitoneal (i.p.) administration with a 1-ml syringe and a 26-gauge, 1/2-inch injection needle, or with isoflurane. Perfuse the mouse with 20 ml of cold D-PBS to remove the blood from the organ. Next, perfuse with 20 ml of cold 4% PFA at <10 ml/min. Carefully dissect the whole brain or other organs with scissors and tweezers so as not to damage the sample.
   ! CAUTION All experiments must follow the relevant governmental and institutional guidelines for animal experiments.
   ▲ CRITICAL STEP Cooling of D-PBS and 4% PFA is important for successful perfusion.

Fixation ● Timing 0.5–1 d

2 Fix dissected organs in 10 ml of 4% PFA with gentle shaking at 4 °C for 12–24 h.
   ▲ CRITICAL STEP Keep fixation duration and temperature as specified to avoid overfixation. Overfixation (from, e.g., >2 d of fixation or high temperature) causes lower clearing efficiency.

PBS wash ● Timing 0.5 d

3 To remove the remaining PFA, wash the fixed organs with 10 ml of PBS with 0.01% (wt/vol) sodium azide for at least 2 h twice at room temperature.
   ■ PAUSE POINT The fixed organs can be stored at −80 °C. First, place the organs in 30 ml of 30% (wt/vol) sucrose and gently shake them at 4 °C. After the organs sink to the bottom (will take almost 1 d), put them into OCT compound and store them at −80 °C for up to 6 months. To start the tissue-clearing steps, in order to remove the sucrose and OCT compound, thaw the samples at room temperature and wash with PBS at least twice, with each wash lasting 1 h.

Tissue clearing ● Timing 6–24 d

4 In this step, we describe two tissue-clearing procedures. Option A is a rapid tissue-clearing protocol for highly transparent mouse organs. Option B is a tissue-expansion protocol for high-resolution imaging of mouse organs. These protocols may need some modifications, such as changes in reagent volumes and immersion duration, for application to organs other than brains. The reagent volume and tube size described here are optimized for mouse brain, but the user can modify them appropriately according to organ size.
   (A) **Advanced whole-organ clearing protocol using CUBIC-L and CUBIC-R+**
      (i) *Half-diluted CUBIC-L treatment.* Immerse the fixed organ in 10 ml of half-diluted CUBIC-L with gentle shaking at 37 °C for at least 6 h (Fig. 2b,c). Overnight incubation can also be used. This step may be optional, but we recommend performing this step to prepare highly transparent organs.
      (ii) *CUBIC-L treatment.* Replace the 10 ml of CUBIC-L solution and continue gentle shaking at 37 °C for 2–5 d. Refresh the CUBIC-L every 2 d. After CUBIC-L treatment, all organs should become translucent white.
         ! CAUTION Because CUBIC-treated organs are soft, in order to avoid physical damage, we recommend handling them with round-edged spoons, instead of tweezers.
         ▲ CRITICAL STEP Young mouse brains (e.g., <3 weeks) or small organs are sufficiently delipidated by 2 d of immersion. On the other hand, elderly mouse brain (e.g., >24 weeks) or samples fixed long-term with formalin or PFA (e.g., >1 week) need >5 d of immersion.
      (iii) *PBS wash.* To stop the delipidation reaction and wash out the remaining CUBIC-L reagent, wash the sample with 10 ml of PBS with gentle shaking at room temperature for at least 2 h. Repeat this washing step more than three times.
         ■ PAUSE POINT CUBIC-L-treated organs can be stored at 4 °C for up to 1 week in PBS–0.01% (wt/vol) sodium azide. After storing, you can restart the staining or RI-matching steps without additional procedures.

(iv) *(Optional) Nuclear staining*. Immerse the sample in 10 ml of staining buffer with gentle shaking at room temperature twice for at least 2 h each time. Then replace the staining buffer with staining buffer containing nuclei-staining dye (PI: 30 µg/ml (final concentration), RD2: 20 µl of 200× solution in 3 ml of staining buffer) and continue gentle shaking at 37 °C for 3 d. The reagent volume and concentration can be optimized for the organ size.

! CAUTION Some nuclear staining dyes, such as SYTO16, are incompatible with CUBIC-R + (see Table 1 for guidance).

(v) *(Optional) PBS wash*. Wash the sample with >20 ml of PBS with gentle shaking for at least 2 h. Repeat this washing step more than three times. Overnight washing can alternatively be used.

(vi) *Half-diluted CUBIC-R+ treatment*. Immerse the sample in 5 ml of half-diluted CUBIC-R+ with gentle shaking at room temperature for at least 6 h. Overnight immersion can also be used. The reagent volume and tube size can be adjusted for the organ size.

? TROUBLESHOOTING

(vii) *CUBIC-R+ treatment*. Immerse the sample in 4 ml of CUBIC-R+ in a 5-ml tube and gently shake it at room temperature overnight. The next day, replace the reagent with fresh reagent and incubate for a further 24 h. The reagent volume and tube size can be adjusted for the organ size.

! CAUTION When imaging fluorescent-protein-labeled organs, the signal intensity may decrease in the CUBIC-R+ solution; therefore, long-term storage at this point is not recommended.

? TROUBLESHOOTING

■ PAUSE POINT Organs can be left in CUBIC-R+ at room temperature. The maximum storage period depends on the staining dye. Organs stained with PI and RD2 can be stored for >1 month at room temperature in a dark environment. Avoid storage at 4 °C, so that the samples do not crystallize.

(B) **Whole-organ expansion and clearing protocol using CUBIC-X for high-resolution imaging**

(i) *Half-diluted ScaleCUBIC-1 treatment*. Immerse the fixed organ in 10 ml of half-diluted ScaleCUBIC-1 (50% (vol/vol) ScaleCUBIC-1 and 50% (vol/vol) dH$_2$O) with gentle shaking at 37 °C for at least 3 h. Overnight incubation can also be used.

(ii) *ScaleCUBIC-1 treatment*. Replace the half-diluted ScaleCUBIC-1 solution with 10 ml of ScaleCUBIC-1 solution and gently shake the mixture at 37 °C for 5–14 d. The delipidation solution should be refreshed every 4 d. After ScaleCUBIC-1 treatment, all organs should become translucent white.

! CAUTION When delipidating organs labeled by fluorescent proteins, replace ScaleCU-BIC-1 with modified-ScaleCUBIC-1.

! CAUTION Because CUBIC-treated organs are soft, in order to avoid physical damage, we recommend handling them with round-edged spoons, instead of tweezers.

▲ CRITICAL STEP To avoid the quenching of fluorescent proteins, the delipidation duration is reduced. Typically, we treat for 8 d for mouse brain expressing fluorescent proteins.

(iii) *PBS wash*. Wash as described in Step 4A(iii).

(iv) *(Optional) Nuclear staining*. Stain as described in Step 4A(iv).

(v) *(Optional) PBS wash*. Wash as described in Step 4A(v).

(vi) *CUBIC-X1 treatment*. Immerse the sample in 30 ml of CUBIC-X1 and shake gently at room temperature or 4 °C for 2.5 d. Refresh the CUBIC-X1 solution twice a day (five times in total).

! CAUTION Because the expanded organ is fragile, be careful while handling it in all the following procedures.

▲ CRITICAL STEP We recommend that samples expressing fluorescence protein be incubated at the lower temperature to avoid quenching.

? TROUBLESHOOTING

(vii) *CUBIC-X2 treatment*. Replace the CUBIC-X1 with 30 ml of CUBIC-X2 and continue gentle shaking at room temperature for 1.5 d. Refresh the CUBIC-X2 solution twice a day (three times in total).

5 *Gel embedding*. To mount a CUBIC-R+-treated sample on a customized LSFM, the sample should be embedded in an agarose gel mixed with CUBIC-R+. For a CUBIC-X2-treated sample, CUBIC-X2 must be used instead. Because the illumination laser may be curved at the interface between the gel and the oil, a sample must be embedded at a distance from the surface. The specific gravity of

the gel mixture can change during the gel embedding process because of additional agarose and water evaporation; as a result, the sample can sink or float in the gel mixture and the sample will be embedded near the gel surface. Therefore, a three-layer protocol was developed to avoid the difference in specific gravity between the gel mixture and a sample being an issue (Fig. 2j). For an example of a three-layer protocol using the gel mold (the inner size is 32 mm × 50 mm × 14 mm, Fig. 2h), an adult mouse brain treated with CUBIC-R+ has an ~10-mm thickness, so the length of the top and bottom margins is determined to be 2 mm (margin = (14–10)/2 = 2 mm). Follow option A to embed a clear organ and option B to embed a fluorescent bead gel for calibration purposes.

(A) **Gel embedding for a cleared organ**

(i) *Preparation of agarose–CUBIC reagent*. Before dissolving the agarose, thoroughly diffuse the 2% (wt/wt) agarose powder in CUBIC-R+ at room temperature by vigorous stirring (Fig. 2d). For example, to prepare four samples to be embedded using a gel mold (Fig. 2h), add 3 g of agarose to 147 g of CUBIC-R+ solution in a capped glass bottle. Heat the thoroughly diffused agarose–CUBIC-R+ mixture in a microwave until it starts to boil. Be sure to loosen the bottle cap before heating. Remove the bottle from the microwave, cap the bottle and shake it vigorously. Repeat the microwave heating and shake the bottle several times until the agarose has dissolved completely (Fig. 2d).

! CAUTION Tightly capped bottles should not be heated in the microwave because they may explode.

▲ CRITICAL STEP Checking whether the agarose–CUBIC-R+ mixture becomes transparent is important when determining whether it has dissolved.

▲ CRITICAL STEP Gelation properties of agarose vary depending on the producer. To fully reproduce our results, use appropriate agarose from listed vendors (Nacalai Tesque for CUBIC-R+, Nippon Gene for CUBIC-X). If the combination of CUBIC solution and agarose is not suitable, it will not gel or become transparent. If the recommended agaroses are not available, high-melting-point or high-strength agaroses may be an alternative.

? TROUBLESHOOTING

(ii) *Degassing incubation*. Incubate the agarose–CUBIC-R+ solution bottle in a hot water bath at 60 °C for at least 30 min in order to remove bubbles from the agarose–CUBIC solution (Fig. 2e,f).

(iii) *Preparation of the bottom gel layer*. Transfer 3.2 ml of agarose–CUBIC-R+ solution (corresponding to 2 mm of the gel mold) to each gel mold with a 10-ml pipette. Spread the agarose–CUBIC solution in the gel mold uniformly. Promptly remove any bubbles carefully with a 1-ml micropipette before viscosity increases. Then leave the agarose–CUBIC solution covered with a lid at 4 °C for 20 min. If the agarose–CUBIC solution does not turn into a gel, then incubate at 4 °C for an additional 20 min.

▲ CRITICAL STEP To keep the agarose–CUBIC solution at 60 °C, return the agarose–CUBIC solution bottle to the hot water bath immediately after pouring.

▲ CRITICAL STEP Agarose-CUBIC solution is easily crystallized by water evaporation, so a lid is needed when incubating agarose–CUBIC solution.

▲ CRITICAL STEP Longer incubation times, such as several hours at 4 °C, can make samples crystallize. Timekeeping and frequent checking are essential.

? TROUBLESHOOTING

(iv) *Making of the middle gel layer*. Carefully transfer the cleared samples to a 50-ml tube. Pour 16 ml (corresponding to a 10-mm height of the gel mold) of agarose–CUBIC solution into the 50-ml tube (Fig. 2g). Immediately decant the mixture into the gel mold in a careful manner. Use a spoon to set a sample at the center position and remove any bubbles existing under the sample (Fig. 2i,j). Promptly remove the bubbles carefully with a 1-ml micropipette before gel viscosity increases. Leave the gel mold covered with a lid at 4 °C for 30 min in a place away from light. If the solution cannot turn into a gel, incubate at 4°C for an additional 20 min.

? TROUBLESHOOTING

(v) *Making of the top gel layer*. Decant the agarose–CUBIC solution into a gel mold until the surface protrudes slightly. Remove the bubbles carefully and cover with a top acrylic plate carefully so as not to introduce bubbles inside; incubate at room temperature for at least 6 h.

(vi) *Stick the sample to the sample holder*. Remove the gel from the mold; it should come out easily (Fig. 2k). To mount the sample on a customized LSFM, stick the gel-embedded

sample to the sample holder by using 2% (wt/wt) agarose–dH$_2$O gel as an adhesive (Fig. 2l) and incubate at room temperature for 30 min. 2% (wt/wt) agarose–dH$_2$O gel can be made by dissolving 0.4 g of agarose in 19.6 g of dH$_2$O, using microwave heating.

▲ **CRITICAL STEP** If necessary, make the inner surface of the sample holder (i.e., where the holder touches the gel) uneven to prevent slipping. We use epoxy adhesives to achieve this.

(vii) *RI matching after gel embedding.* Put the gel-embedded sample into a plastic bag with a zipper and add enough CUBIC-R+ or CUBIC-X2 to immerse it.

▲ **CRITICAL STEP** This incubation step recovers the transparency of the samples by matching the RIs of the sample to that of the gel.

■ **PAUSE POINT** Gel-embedded organs stained with PI and RD2 can be stored for >1 month at room temperature in the dark. Avoid storing at 4 °C so that the samples will not crystallize.

(B) **Calibration gel preparation**

(i) For fluorescent bead gel preparation, dissolve 4% (wt/wt) agarose powder in 96% (wt/wt) CUBIC-R+ agarose and incubate at 60 °C as described in Step 5A(i,ii).

(ii) Diffuse Sphero fluorescent particles into CUBIC-R+ and mix with an equal amount of CUBIC-R+–4% (wt/wt) agarose solution at room temperature. For example, typically, 5 μl of fluorescent beads (Sphero fluorescent particles, purple, 0.1–0.3 μm, 1.0% (wt/vol)) are diffused into 7.5 g of CUBIC-R+ and mixed with 7.5 g of CUBIC-R+–4% (wt/wt) agarose solution.

(iii) Transfer the fluorescent beads diffused in CUBIC-R+–2% (wt/wt) agarose solution into an appropriate mold and allow the solution to gel as described in Step 5A.

? **TROUBLESHOOTING**

Imaging of the cleared organ with light-sheet fluorescence microscopy ● Timing 2–12 h per sample

▲ **CRITICAL** To image the cleared organ at single-cell resolution, we used a customized LSFM, which we describe in detail below. Alternative imaging systems can be used in place of this. A tiling scheme was introduced because the field of view is limited in the *x–y* plane. For example, an adult mouse whole-brain sample cleared by CUBIC-R+ is usually separated into 11–15 tiles in the *x* direction and 14–20 tiles in the *y* direction with sufficient overlap. Each tile is scanned in the *z* direction for up to a 7.5-mm thickness, and the distance per acquisition cycle is set to 5 μm. After one tile is finished, the field of view is moved to another tile position and the scan is started in the *z* direction. This is repeated until all tiles have been completed. In addition, to cover a thick organ in the *z* direction, the sample is rotated by 180°, and then the opposite side of the sample is imaged using the same tiling scheme as that used for the 0° side (Fig. 3d). The acquisition sequence can be controlled by LabVIEW and Visual Studio C#.

6 *Setting a gel sample for microscopy.* Fix the sample to the *θ* stage through the sample holder after removing the excess CUBIC reagent on the surface (Fig. 3b,c). Typically, we wipe the sample softly with lint-free tissue and dip it into the RI-adjusted oil mix several times.

7 *x–y–z–θ positioning.* To acquire whole-organ images using the imaging system with a limited field of view and WD of the detection objective, we suggest *x–y* positioning at first. Define the *x–y* position arrays of the imaging region by identifying the start and end positions of both the *x* direction and *y* direction with changing *z* positions and searching the edge of a sample in the *x–y* plane. Calculate the *x–y* position arrays on the basis of the effective imaging area determined by the field of view of the objective (in this setup, *x* = 1.40 mm and *y* = 1.66 mm) and the appropriate overlap value (130-μm overlap for both *x* and *y* axes).The overlap value is defined to ensure that there will not be any loss of sample regions.

▲ **CRITICAL STEP** To avoid signal quenching, the laser power must be weakened during the adjustment of position and focus. For example, we use 2 mW for the 594-nm laser for adjustment and 500 ms of exposure time, as compared with 20 mW for image acquisition and 20–50 ms of exposure time.

▲ **CRITICAL STEP** The accuracy and straightness of the *x–y–z–θ* stage must be taken into consideration for overlap value.

▲ **CRITICAL STEP** The left and right halves of the sample should be illuminated by the left and right illumination arms, respectively, for homogeneous illumination intensity.

8 Next, carry out *z–θ* positioning. When imaging thick organs, which are larger than the WD of the detection objective lens, we use rotation sequences. Rotate the sample along the *y* axis and

determine the center of rotation in the x–z plane manually by searching identical structures from the $\theta = 0°$ and $\theta = 180°$ sides. Set the z start position with an appropriate overlap value for the z axis, and merge the two sides of the image blocks continuously.

! CAUTION Be careful not to hit the chamber with the sample. θ-stage rotation must be performed at a sufficient distance from the chamber wall.

9 *Set the laser setting.* Typically, the excitation laser power is 20 mW (measured at each side of the laser illumination before the illumination objective lens) and the exposure time is 20–50 ms. However, the exposure times may have to be adjusted, depending on the fluorescence signal intensities of sample.

! CAUTION Strong lasers may cause photobleaching of samples during imaging.

10 Check two images by dual-color imaging in order to merge them completely. The fluorescent beads (Sphero fluorescent particles) can be used for the calibration of dual-color imaging by 488-, 594-, and 642-nm lasers, a dichroic mirror, a 625-nm band-pass filter and a 720-nm long-pass filter.

11 Set an appropriate threshold for MOVIE-skip. Typically, we use two times the value of the mean intensity of the image in the blank region, but it depends on the signal intensity. Set the initial light-sheet position for MOVIE-focus automatically for each stack, as follows: typically, 20 images separated by 3.5 μm are acquired (thus the total range is 66.5 μm), and the best light-sheet position is determined by evaluating DCTS scores.

12 *Acquire images.* When using the MOVIE system, the system can run as fast as 18–40 fps per color (Fig. 4b). Acquire images and save appropriately. Each image size is ~11 MB (2,160 × 2,560 pixels, 16 bits per pixel), and we transfer them to the server and save them to hard disks or SSDs in real time through a 56-Gbps InfiniBand system. Each stack (one color, one x–y position) is saved to a different folder and folders of the same y position are located in the same directory. The hierarchy and folder names are used in downstream data analysis. The total image acquisition of CUBIC-R +-treated whole mouse brain should be completed within 2–5 h, yielding ~360,000 images (4–5 TB of data) with the MOVIE system.

▲**CRITICAL STEP** Keep the microscopy room dark to decrease the background. The MOVIE system may be susceptible to background change.

? TROUBLESHOOTING

Cell-nucleus detection ● Timing 2–8 h per sample

▲**CRITICAL** For quantitative characterization of the sample, we implemented an informatics pipeline to detect cell nuclei in the acquired images. To reduce labor and time, the algorithm is designed to work with less manual preparation and is more time efficient while maximizing accuracy as much as possible. We implemented the image-processing program by CUDA, C++ and Python. All the settings and parameters should be provided as a JSON text file. This parameter file includes imaging-related settings (image size, overlap size, pixel size in micrometers and file naming conventions) and algorithmic parameters (sets of filter sizes for image processing and threshold values for suppressing obviously noisy candidates). The processing time can vary according to different computer specifications. In the following, we denote the Python scripts in the 'script' directory in the provided code set with a '`.py`' extension and the parameter files in the 'param' directory with a '`.json`' extension.

13 *Software setup.* In this step, download and install the requisite programs. First, download the source code by running the following command:

```
git clone https://github.com/lsb-riken/CUBIC-informatics
```

Then build the source code. To build the programs under the 'build' directory, run the following commands in the 'CUBIC-informatics' directory.

```
mkdir build
cd build
cmake -DCMAKE_BUILD_TYPE=Release -DCMAKLE_INSTALL_PREFIX=. ..
make
make install
```

If the necessary software programs (Software and tools), including the CUDA Toolkit, are installed correctly, it will finish within a few minutes without any error messages in the output. In addition, install the required Python libraries by running the following command in the 'CUBIC-informatics' directory:

```
pip install -r requirements.txt
```

14 *Parameter file preparation.* Before running the programs, prepare the parameter files. The tiling check, cell candidate detection and candidate verification (Steps 15–17) for one organ require two image sets ($\theta = 0°$, 180°) and four parameter files, which we call HDoG_FW, HDoG_RV, Merge and Classify. Both the HDoG_FW (for $\theta = 0°$) and HDoG_RV (for $\theta = 180°$) parameter files should specify the settings for the source and destination directories, GPU identifications (IDs) to be used, input image specification (image size and margin in pixels), coordinate information (pixel size in micrometers and relative position of origin in global coordinates) and the algorithmic parameters (normalization filter size, 3D-DoG filter size, and other minor parameters) for HDoG_gpu.py. The Merge parameter file should specify the destination directory, FW/RV boundary positions, whether or not to rotate and flip before tiling, downscaled voxel size in micrometers and whether or not to flip after tiling. The Classify parameter file should specify the destination directory and coefficients of the decision boundary line. Example parameter files and detailed descriptions of each parameter are provided in param_example_HDoG_FW.json, param_example_HDoG_RV.json, param_example_ mergebrain.json and param_example_classify.json which are included in the 'param' directory of our CUBIC-informatics program. For second-channel verification, in addition to the same set of four parameter files for the second-channel images, a MultiChannel parameter file is required, whose example is provided as param_example_multichannel.json.

15 *Tiling check (MergeBrain.py).* Before cell-nucleus detection, to check if any issues arose during the imaging steps, such as missing images or stacks, downscale the acquired x–y tile images (from $0.65 \times 0.65 \times 5$ μm/voxel to $13 \times 13 \times 10$ μm/voxel) and reconstitute to a whole-organ image in 16-bit TIFF format by using the MergeBrain.py script. Run the following command, replacing the parameter file name with the one you specified in the previous step.

```
python script/MergeBrain.py images param/param_example_mergebrain.json
```

This program can convert 1 TB of image data to 2.5 GB of image data in <30 min. It allows the images to be rotated and flipped before being appended so that the x–y tile will be correctly aligned. Check whether x–y tile images have been properly acquired by using visualization software such as ImageJ. If an improper stack is found, it is necessary to acquire the stack again. By using x–y tile images, the 3D reconstitutions can be visualized with the Imaris software (Fig. 3e).

16 *Cell candidate detection (HDoG_gpu.py, MergeBrain.py).* To extract the cell candidates from the raw image data, process the images by normalizing signal intensities, applying a 3D-HDoG filter and labeling connected components by running HDoG_gpu.py, followed by MergeBrain.py, to merge the results of the $\theta = 0°$ and 180° image sets and transform cell positions in the whole-organ coordinate system. Run the following commands, replacing the parameter file name with the one you specified in Step 14.

```
python script/HDoG_gpu.py param/param_example_HDoG_FW.json
python script/HDoG_gpu.py param/param_example_HDoG_RV.json
python script/MergeBrain.py cells param/param_example_mergebrain.json
```

The cell-nucleus-detection pipeline extracts cell-like objects from images using GPUs. This step takes the longest time in the pipeline, but it can be shortened if multiple GPUs are available. With four GPUs, we found that the system processed ~2 TB/h. When the program finishes, it outputs a collection of centroid positions and regional features for each cell candidate region (3–12 GB), which are used in the next step.

▲ **CRITICAL STEP** Voxel values are normalized using the minimum and maximum intensity of the surrounding $65 \times 65 \times 40$-μm range, but the normalization kernel size can also be changed by parameter file modification. If the size is too small, the normalization process may produce a false patterns, whereas it is computationally intensive to use a large kernel size. To avoid artifacts and finish this process quickly, the optimization of the size is important.

▲ **CRITICAL STEP** Users should choose appropriate 3D-DoG (scale) parameters for accurate cell-nucleus detection because this step is dependent on the physical and optical magnification. The parameter can be adjusted easily by using the HDoG_intermediate.py script. We set the 3D-DoG filter sizes as $\sigma_{xy(\text{large})} = 4.875$ (7.5), $\sigma_{z(\text{large})} = 11.25$ (2.25) and $\sigma_{xy(\text{small})} = 3.25$ (5.0), $\sigma_{z(\text{small})} = 7.5$ (1.5) μm (pixel) for the CUBIC-X mouse brain and $\sigma_{xy(\text{large})} = 3.9$ (6.0), $\sigma_{z(\text{large})} = 7.5$ (1.5) and $\sigma_{xy(\text{small})} = 2.5$ (4.0), $\sigma_{z(\text{small})} = 5.0$ (1.0) μm (pixel) for the CUBIC-R+ mouse brain.

17　*Candidate verification (HDoG_classifier.py)*. In this step, each cell candidate is classified as either a real cell or just noise according to its features (maximum intensity in the region and regional structureness). Run the following command, replacing the parameter file name with the one you specified in Step 14.

```
python script/HDoG_classify.py param/param_example_classify.json
```

This program outputs a classifier file to be used in subsequent steps and plots cell candidate points in 2D feature space. In most cases, real cells and noisy regions show clear separation in feature space. Each cell candidate is classified according to at which side of the decision boundary its feature point is located. Define an appropriate decision boundary by looking at feature space distribution and set it in the parameter file. We use the following linear decision boundary for most samples: $6.0\,X_1 + 0.75\,X_2 + 1 = 0$. Note that X_1 is the logarithm of maximum intensity and X_2 is the logarithm of structureness (Fig. 7).

18　*Second-channel verification (MultiChannelVerification.py)*. In addition to nuclear staining images for the first channel, use images of other channels to detect any cell signals. Run the following command:

```
python    script/MultiChannelVerification.py    param/param_example_
multichannel.json
```

Based on the position of a cell from the first channel, we can judge whether it has a positive signal or not, by comparing the corresponding intensity in the second channel. For AAV-PHP.eB:NSE-H2B-mCherry-infected samples, we computed the ratio of log intensity between mCherry and RD2 at the centroid of the cells. We set the threshold manually and also performed unsupervised clustering to distinguish the positive from the negative cells. These two methods produced similar results, and we used 1.0 as the threshold for the ratio of log intensity.

▲ **CRITICAL STEP** We used the intensity ratio because the raw intensity value is affected by the strength of the excitation laser, which is not uniform over the whole brain.

? **TROUBLESHOOTING**

Alignment and annotation ● Timing 1–8 h per sample

▲ **CRITICAL** To quantify the number of cells in each anatomical region, use the mouse brain atlas (CUBIC-Atlas) and a program for mapping (AtlasMapping.py). Mapping is performed in two stages. The first stage is image-based registration to the reference and the second stage is point-based annotation using the atlas ID. We implemented the mapping tool with Python. Of course, this program can also be used to align other organs, using an appropriate reference organ image, but in such cases, it cannot perform the annotation step.

19　*Reference data and parameter file preparation*. First, prepare the reference data. For mouse brain, download the CUBIC-Atlas reference data from http://cubic-atlas.riken.jp/, which include reference images and point-based annotation data. For other organs, prepare the appropriate reference images by yourself. Next, create a parameter file for the registration and annotation step, whose example is provided as param_example_mapping.json in the 'param' directory of our CUBIC-informatics program. It should contain the destination directory, the installed ANTs directory, the installed CUBIC-Atlas directory, the path to classifier file produced in the candidate verification step, the voxel size in the ANTs registration and the maximum distance for a transformed detected cell to be annotated with the ID of the nearest reference point.

20　*Registration (AtlasMapping.py)*. Before annotation, register the nuclear-stained whole-brain image to the reference image of the CUBIC-Atlas by running following command.

```
python    script/AtlasMapping.py    registration    param/param_example_
mapping.json
```

It calls the ANTs registration command with our recommended parameters. We provide reference images in 40- and 80-μm voxel sizes. We mainly use 80-μm voxel images for quick registration (about 1 h). Because this step does not require the results of cell-nucleus detection, the cell-nucleus-detection steps and this step can be performed simultaneously if the computer has enough capacity (CPU cores and RAM).

21 *Annotation (AtlasMapping.py)*. Map cell positions to the atlas coordinate system by applying nonlinear transformations obtained in the previous step and assign the atlas ID of the nearest reference point for each detected cell. Run the following command.

```
python script/AtlasMapping.py annotation param/param_example_map-
ping.json
```

This annotation step should take about 10 min. Because the cell detection step tends to detect bubbles or dust outside the organ, we assign ID = 0 to the detected cells far from any of the reference points in CUBIC-Atlas. We use 160 μm as the maximum distance, but this can be adjusted in the parameter file.

? TROUBLESHOOTING

Troubleshooting

Troubleshooting advice can be found in Table 2.

Table 2 | Troubleshooting table

Step	Problem	Possible reason	Solution
Reagent setup	Undissolved solute remaining in CUBIC-R+ or CUBIC-X2 reagent	Reduction of solubility by heat of dissolution	Use mild heating and mix with a stirrer or use overnight stirring at room temperature
	Crystallization of CUBIC-R+ or CUBIC-X2 reagent	Water evaporation or decreasing temperature	Check and adjust the temperature and RI value with dH$_2$O
Equipment setup	Entirely unmatched fields of view from two sCMOS cameras	Misalignment of the dichroic mirror	Adjust the position and angle of the dichroic mirror with a kinematic mount
		Chromatic aberration	Correct by extending or shortening the distance between tube lens and the sCMOS camera
	Diminishing of signals at the periphery	Clipping of the collected photon by the dichroic mirror, tube lens, or filters after detecting objective lens	Align them closely as much as possible, or replace them with larger ones
4A(vi,vii)	Poor organ clearing	Insufficient incubation in CUBIC-L or Sca*l*eCUBIC-1	Increase delipidation time
		Insufficient RI matching	Exchange the CUBIC-R+ or CUBIC-X2 more than once or twice additionally
4B(vi))	Poor organ swelling	Insufficient incubation in CUBIC-X1	Increase the length of the swelling step with CUBIC-X1
5A(i,iii,iv), 5B(iii)	Solution does not become a solid gel	Not using appropriate agarose for CUBIC reagent	Try 1–3% (wt/wt) high-melting-point or high-strength agarose
	Bubbles in the agarose–CUBIC solution when gel-embedding	Increased viscosity of agarose–CUBIC solution	Agarose–CUBIC solution becomes more viscous at room temperature; hence, the bubbles have to be removed until the gel solidifies. Be careful of bubbles at the border and corner of the gel mold, because these are harder to find
	Gel becomes cloudy white	Recrystallization of solute	CUBIC-R+ or CUBIC-X2 is easily crystalized when cooling. Perform a 4 °C incubation for <30 min
			Incubation in CUBIC-R+ or CUBIC-X2 warmed at 60 °C. The crystal will be dissolved
6–12	Inhomogeneous nuclear signal	Insufficient penetration of nuclear-staining dye	Increase the staining time or optimize the staining conditions
	Weak or non-detectable fluorescent protein signals	Quenching of fluorescent protein	Use CUBIC-R+(M) for RI matching
			Decrease the incubation temperature for all steps
		Insufficient fluorescence signal	Choose bright fluorescent protein expression system by using a strong expression promoter

Table 2 (continued)

Step	Problem	Possible reason	Solution
	High autofluorescence	Insufficient delipidation	Increase CUBIC-L or ScaleCUBIC-1 treatment time
	Poor z-resolution	Wrong setting of the light-sheet position	Adjust the light-sheet distance from the detection objective lens
		Laser is too thin before illumination objective lens	Expand the illumination laser diameter
	Shade inside the sample	Obstruction, such as bubbles, crystallized CUBIC reagents and dust	Remove the obstruction
			Increase the amplitude of the y-galvo
		Light absorption by high-cell-density region	Try staining with a lower concentration of dye
	Defocus	Wrong combination of immersion oil and CUBIC reagents	Use appropriate oil. For CUBIC-R+, completely mix HIVAC F-4 (RI = 1.555) and mineral oil (RI = 1.467) in a 3:2 ratio with a stirrer. The mixture's RI is 1.522, comparable to that of CUBIC-R+. For CUBIC-X2, use a mineral oil (RI = 1.467)
		Mismatch between the update timing of light-sheet position and image analysis of MOVIE-focus	Synchronize the timing of the z-galvo and sCMOS cameras
	Lack of images near the edges of the sample	Incorrect specification of the acquisition area	Determine the xy range of the sample region carefully, while changing the z-position
	Low effect of MOVIE-skip	Wrong threshold used in MOVIE-skip	Change the threshold of MOVIE-skip, and check the whole-organ coverage
		MOVIE-skip detects the intensity of particles of dust outside the sample	Optimize the block size (typically, we use 40 × 40 pixel blocks), corresponding to the particle size
	Image save error	Insufficient network communication speed	Use a 56-Gbps InfiniBand system, directly transferring data to storage in the server. Make a program to reacquire the stack of images when unexpected errors happen. The remote Windows10 desktop may disturb network communication; therefore, turn it off during imaging
16–18	Incorrect tile images	Wrong parameters used for MergeBrain.py	Change the options to rotate or flip the images before tiling. Check the boundary position of the front side and the back side
	Inappropriate detection (overcounting or undercounting)	Weak or nondetectable fluorescence	Increase the exposure time and laser power of the imaging condition
		Filter size is too small for intensity normalization	Run HDoG_intermediate.py, check the extracted region and optimize the parameters
		Complex morphology	This algorithm is optimized for sphere-signal detection. Samples must be prepared to be suitable for this algorithm
	Inappropriate detection (undercounting)	Oversuppression of noisy regions	Check the maximum intensity and volume of the cells in the images. Too high a threshold value will discard the true cells
	Overcounting and multiple detection of single cells	Scale parameter is too small	Run HDoG_intermediate.py, check the extracted region and optimize the parameters
	Undercounting and single detection for multiple cells	Scale parameter is too large	Run HDoG_intermediate.py, check the extracted region and optimize the parameters
	Inappropriate verification (overcounting or undercounting)	Decision boundary is wrong	Plot cell candidate point in images according to the feature value. It may help in understanding the relationship between image and feature. Then set the decision boundary manually to optimize the performance
19–21 (alignment and annotation)	Wrong registration result	Downscaled image is not in the same scale as the reference image	Check the scale after downscaling in the parameter for MergeBrain.py and the scale of reference in the parameter for AtlasMapping.py
		Downscaled image is not in the same orientation as the reference image	Plot the 3D downscaled image with ImageJ or Imaris and check that the orientation of the sample is almost the same as the reference image. If not, change the parameter for AtlasMapping.py by flipping or rotating

Timing

Step 1, dissection: 10–15 min
Step 2, fixation: 0.5–1 d
Step 3, PBS wash: 0.5 d
Step 4A(i–iii), delipidation: 3–6 d
Step 4A(iv,v), (optional) nuclear staining: 4 d
Step 4A(vi,vii), RI matching: 2 d
Step 4B(i–iii), delipidation: 6–15 d
Step 4B(iv,v), (optional) nuclear staining: 4 d
Step 4B(vi), swelling: 2.5 d
Step 4B(vii), RI matching: 1.5 d
Step 5, gel embedding: 1 d
Steps 6–12, imaging: 2–12 h per sample
Steps 13–18, cell-nucleus detection: 2–8 h per sample
Steps 19–21, alignment and annotation: 1–8 h per sample

Anticipated results

The CUBIC protocol can be used to prepare highly transparent (Step 4A; CUBIC-L/R+) or expanded (Step 4B; CUBIC-X) organs with good retention of fluorescent protein signal with simple immersion procedures. These transparent organs can be imaged by a conventional or customized LSFM. After the tissue-clearing procedure using the CUBIC-L/R+ protocol, highly transparent whole mouse brains with strong signals of the fluorescent protein mCherry can be obtained (Fig. 3e). If using a poorly cleared organ, the images of the deep regions become dark and blur. When the CUBIC-X protocol is used for a whole brain, it will be expanded about 2.2-fold and can generate high-resolution images. The images of CUBIC-L/R+-treated whole mouse brains can be acquired in about 24 h by a classic stop-and-exposure scheme with ~6 TB of data/color. On the other hand, the MOVIE system can reduce the acquisition time to 5 h (2.5 TB of data/color × 2 colors) for CUBIC-L/R+-treated whole mouse brains.

Whole-organ scale data can be efficiently analyzed at a data throughput of 2 TB/h by the 3D-HDoG-based cell-nucleus-detection algorithm using multiple-GPUs and multiple-CPU processing. The F-scores of cell-nucleus detection should be more than 90% for a CUBIC-X-treated whole mouse brain and, except in high-cell-density regions such as the cerebellum and olfactory bulb, for a CUBIC-R+-treated mouse brain (Fig. 8b,c). Furthermore, the 3D-HDoG-based cell-nucleus-detection algorithm, when combined with dual-color imaging, can rapidly and accurately obtain information about the cellular state. Because this point-based organ analysis can reduce the data size, downstream analysis will become much simpler and it is easier to handle the entire raw dataset. Our future biomedical studies will further develop and investigate this point-based concept.

Reporting Summary

Further information on research design is available in the Nature Research Reporting Summary linked to this article.

Data availability

CUBIC-Atlas v.1.2 reference data are available from http://cubic-atlas.riken.jp. Other datasets generated or analyzed during the current study are available from the corresponding author upon reasonable request.

Code availability

All source code and a brief guide for data analysis are available on https://github.com/lsb-riken/CUBIC-informatics. Source code for the microscope and MOVIE system is available from the corresponding author upon reasonable request.

References

1. Voie, A. H., Burns, D. H. & Spelman, F. A. Orthogonal-plane fluorescence optical sectioning: three-dimensional imaging of macroscopic biological specimens. *J. Micros.* **170**, 229–236 (1993).

2. Keller, P. J., Schmidt, A. D., Wittbrodt, J. & Stelzer, E. H. Reconstruction of zebrafish early embryonic development by scanned light sheet microscopy. *Science* **322**, 1065–1069 (2008).

3. Huisken, J., Swoger, J., Del Bene, F., Wittbrodt, J. & Stelzer, E. H. K. Optical sectioning deep inside live embryos by selective plane illumination microscopy. *Science* **305**, 1007–1009 (2004).

4. Dodt, H. U. et al. Ultramicroscopy: three-dimensional visualization of neuronal networks in the whole mouse brain. *Nat. Methods* **4**, 331–336 (2007).

5. Kim, Y. et al. Mapping social behavior-induced brain activation at cellular resolution in the mouse. *Cell Rep.* **10**, 292–305 (2015).

6. Tomer, R. et al. SPED light sheet microscopy: fast mapping of biological system structure and function. *Cell* **163**, 1796–1806 (2015).

7. Kubota, S. I. et al. Whole-body profiling of cancer metastasis with single-cell resolution. *Cell Rep.* **20**, 236–250 (2017).

8. Nojima, S. et al. CUBIC pathology: three-dimensional imaging for pathological diagnosis. *Sci. Rep.* **7**, 9269 (2017).

9. Glaser, A. K. *et al.* Light-sheet microscopy for slide-free non-destructive pathology of large clinical specimens. *Nat. Biomed. Eng.* **1**, 0084 (2017).

10. Tainaka, K. et al. Chemical landscape for tissue clearing based on hydrophilic reagents. *Cell Rep.* **24**, 2196–2210.e9 (2018).

11. Murakami, T. C. et al. A three-dimensional single-cell-resolution whole-brain atlas using CUBIC-X expansion microscopy and tissue clearing. *Nat. Neurosci.* **21**, 625–637 (2018).

12. Spalteholz, W. *Über das Durchsichtigmachen von menschlichen und tierischen Präparaten.* (S. Hirzel, 1914).

13. Erturk, A. et al. Three-dimensional imaging of the unsectioned adult spinal cord to assess axon regeneration and glial responses after injury. *Nat. Med.* **18**, 166–171 (2011).

14. Erturk, A. et al. Three-dimensional imaging of solvent-cleared organs using 3DISCO. *Nat. Protoc.* **7**, 1983–1995 (2012).

15. Pan, C. et al. Shrinkage-mediated imaging of entire organs and organisms using uDISCO. *Nat. Methods* **13**, 859–867 (2016).

16. Chung, K. et al. Structural and molecular interrogation of intact biological systems. *Nature* **497**, 332–337 (2013).

17. Hogervorst, J. G., Schouten, L. J., Konings, E. J., Goldbohm, R. A. & van den Brandt, P. A. A prospective study of dietary acrylamide intake and the risk of endometrial, ovarian, and breast cancer. *Cancer Epidemiol. Biomark. Prev.* **16**, 2304–2313 (2007).

18. Tomer, R., Ye, L., Hsueh, B. & Deisseroth, K. Advanced CLARITY for rapid and high-resolution imaging of intact tissues. *Nat. Protoc.* **9**, 1682–1697 (2014).

19. Yang, B. et al. Single-cell phenotyping within transparent intact tissue through whole-body clearing. *Cell* **158**, 945–958 (2014).

20. Park, Y.-G. et al. Protection of tissue physicochemical properties using polyfunctional crosslinkers. *Nat. Biotechnol.* **37**, 73 (2018).

21. Bakutkin, V. V., Maksimova, I. L., Semyonova, T. N., Tuchin, V. V. & Kon., I. L. Controlling of optical properties of sclera. *Proc. SPIE* **2393**, 137–141 (1995).

22. Tuchin, V. V. et al. Light propagation in tissues with controlled optical properties. *J. Biomed. Opt.* **2**, 401–417 (1997).

23. Tuchin, V. V. Light scattering of tissues. *Physic* **40**, 495–515 (1997).

24. Tuchin, V. V. Optical clearing of tissues and blood using the immersion method. *J. Phys. D. Appl. Phys.* **38**, 2497–2518 (2005).

25. Hama, H. et al. Scale: a chemical approach for fluorescence imaging and reconstruction of transparent mouse brain. *Nat. Neurosci.* **14**, 1481–1488 (2011).

26. Ke, M. T., Fujimoto, S. & Imai, T. SeeDB: a simple and morphology-preserving optical clearing agent for neuronal circuit reconstruction. *Nat. Neurosci.* **16**, 1154–1161 (2013).

27. Susaki, E. A. et al. Whole-brain imaging with single-cell resolution using chemical cocktails and computational analysis. *Cell* **157**, 726–739 (2014).

28. Hama, H. et al. ScaleS: an optical clearing palette for biological imaging. *Nat. Neurosci.* **18**, 1518–1529 (2015).

29. Perbellini, F. et al. Free-of-acrylamide SDS-based tissue clearing (FASTClear) for three dimensional visualization of myocardial tissue. *Sci. Rep.* **7**, 5188 (2017).

30. Tainaka, K. et al. Whole-body imaging with single-cell resolution by tissue decolorization. *Cell* **159**, 911–924 (2014).

31. Liu, Y. C. & Chiang, A. S. High-resolution confocal imaging and three-dimensional rendering. *Methods* **30**, 86–93 (2003).

32. Helmchen, F. & Denk, W. Deep tissue two-photon microscopy. *Nat. Methods* **2**, 932–940 (2005).

33. Silvestri, L., Bria, A., Sacconi, L., Iannello, G. & Pavone, F. S. Confocal light sheet microscopy: micron-scale neuroanatomy of the entire mouse brain. *Opt. Express* **20**, 20582–20598 (2012).

34. Seiriki, K. et al. High-speed and scalable whole-brain imaging in rodents and primates. *Neuron* **94**, 1085–1100.e6 (2017).

35. Keller, P. J. & Ahrens, M. B. Visualizing whole-brain activity and development at the single-cell level using light-sheet microscopy. *Neuron* **85**, 462–483 (2015).

36. Helmstaedter, M. & Mitra, P. P. Computational methods and challenges for large-scale circuit mapping. *Curr. Opin. Neurobiol.* **22**, 162–169 (2012).

37. Ahrens, M. B., Orger, M. B., Robson, D. N., Li, J. M. & Keller, P. J. Whole-brain functional imaging at cellular resolution using light-sheet microscopy. *Nat. Methods* **10**, 413–420 (2013).

38. Portugues, R., Feierstein, C. E., Engert, F. & Orger, M. B. Whole-brain activity maps reveal stereotyped, distributed networks for visuomotor behavior. *Neuron* **81**, 1328–1343 (2014).

39. Renier, N. et al. iDISCO: a simple, rapid method to immunolabel large tissue samples for volume imaging. *Cell* **159**, 896–910 (2014).

40. Amat, F. et al. Efficient processing and analysis of large-scale light-sheet microscopy data. *Nat. Protoc.* **10**, 1679–1696 (2015).

41. Menegas, W. et al. Dopamine neurons projecting to the posterior striatum form an anatomically distinct subclass. *eLife* **4**, e10032 (2015).

42. Susaki, E. A. & Ueda, H. R. Whole-body and whole-organ clearing and imaging techniques with single-cell resolution: toward organism-level systems biology in mammals. *Cell Chem. Biol.* **23**, 137–157 (2016).

43. Tsai, P. S. et al. Correlations of neuronal and microvascular densities in murine cortex revealed by direct counting and colocalization of nuclei and vessels. *J. Neurosci.* **29**, 14553–14570 (2009).

44. Quan, T. et al. NeuroGPS: automated localization of neurons for brain circuits using L1 minimization model. *Sci. Rep.* **3**, 1414 (2013).

45. Latorre, A., Alonso-Nanclares, L., Muelas, S., Peña, J.-M. & Defelipe, J. 3D segmentations of neuronal nuclei from confocal microscope image stacks. *Front. Neuroanat.* **7**, 49 (2013).

46. Frasconi, P. et al. Large-scale automated identification of mouse brain cells in confocal light sheet microscopy images. *Bioinformatics* **30**, i587–i593 (2014).

47. Amat, F. et al. Fast, accurate reconstruction of cell lineages from large-scale fluorescence microscopy data. *Nat. Methods* **11**, 951–958 (2014).

48. Wu, J. et al. 3D BrainCV: simultaneous visualization and analysis of cells and capillaries in a whole mouse brain with one-micron voxel resolution. *NeuroImage* **87**, 199–208 (2014).

49. Quan, T. et al. Digital reconstruction of the cell body in dense neural circuits using a spherical-coordinated variational model. *Sci. Rep.* **4**, 4970 (2014).

50. Silvestri, L. et al. Quantitative neuroanatomy of all Purkinje cells with light sheet microscopy and high-throughput image analysis. *Front. Neuroanat.* **9**, 68 (2015).

51. Kim, Y. et al. Brain-wide maps reveal stereotyped cell-type-based cortical architecture and subcortical sexual dimorphism. *Cell* **171**, 456–469.e22 (2017).

52. Furth, D. et al. An interactive framework for whole-brain maps at cellular resolution. *Nat. Neurosci.* **21**, 139–149 (2018).

53. Xing, F. & Yang, L. Robust nucleus/cell detection and segmentation in digital pathology and microscopy images: a comprehensive review. *IEEE Rev. Biomed. Eng.* **9**, 234–263 (2016).

54. Zhang, M., Wu, T. & Bennett, K. M. Small blob identification in medical images using regional features from optimum scale. *IEEE Trans. Biomed. Eng.* **62**, 1051–1062 (2015).

55. Theer, P., Mongis, C. & Knop, M. PSFj: know your fluorescence microscope. *Nat. Methods* **11**, 981–982 (2014).

56. Kanda, T., Sullivan, K. F. & Wahl, G. M. Histone-GFP fusion protein enables sensitive analysis of chromosome dynamics in living mammalian cells. *Curr. Biol.* **8**, 377–385 (1998).

57. Chan, K. Y. et al. Engineered AAVs for efficient noninvasive gene delivery to the central and peripheral nervous systems. *Nat. Neurosci.* **20**, 1172–1179 (2017).

58. Shinohara, Y. et al. Effects of neutralizing antibody production on AAV-PHP.B-mediated transduction of the mouse central nervous system. *Mol. Neurobiol.* **56**, 4203–4214 (2018).

59. Sun, Y., Duthaler, S. & Nelson, B. J. Autofocusing in computer microscopy: selecting the optimal focus algorithm. *Microsc. Res. Tech.* **65**, 139–149 (2004).

60. Royer, L. A. et al. Adaptive light-sheet microscopy for long-term, high-resolution imaging in living organisms. *Nat. Biotechnol.* **34**, 1267–1278 (2016).

61. Ryan, D. P. et al. Automatic and adaptive heterogeneous refractive index compensation for light-sheet microscopy. *Nat. Commun.* **8**, 612 (2017).

62. Silvestri, L. *et al.* RAPID: real-time image-based autofocus for all wide-field optical microscopy systems. Preprint at bioRxiv, https://www.biorxiv.org/content/10.1101/170555v1 (2017).

63. Royer, L. A., Lemon, W. C., Chhetri, R. K. & Keller, P. J. A practical guide to adaptive light-sheet microscopy. *Nat. Protoc.* **13**, 2462–2500 (2018).

64. Lindeberg, T. Feature detection with automatic scale selection. *Int. J. Comput. Vis.* **30**, 79–116 (1998).

65. Hawick, K. A., Leist, A. & Playne, D. P. Parallel graph component labelling with GPUs and CUDA. *Parallel Comput.* **36**, 655–678 (2010).

66. Soh, Y., Ashraf, H., Hae, Y. & Kim, I. Fast parallel connected component labeling algorithms using CUDA based on 8-directional label selection. *Int. J. Latest Res. Sci. Technol.* **3**, 187–190 (2014).

67. Frangi, A. F., Niessen, W. J., Vincken, K. L. & Viergever, M. A. Multiscale vessel enhancement filtering. In *Medical Image Computing and Computer-Assisted Intervention — MICCAI'98*, 130-137 (Springer, 1998).

68. Avants, B. B. et al. A reproducible evaluation of ANTs similarity metric performance in brain image registration. *NeuroImage* **54**, 2033–2044 (2011).

69. Pende, M. et al. High-resolution ultramicroscopy of the developing and adult nervous system in optically cleared Drosophila melanogaster. *Nat. Commun.* **9**, 4731 (2018).
70. Konno, A. & Okazaki, S. Aqueous-based tissue clearing in crustaceans. *Zool. Lett.* **4**, 13 (2018).
71. Kurihara, D., Mizuta, Y., Sato, Y. & Higashiyama, T. ClearSee: a rapid optical clearing reagent for whole-plant fluorescence imaging. *Development* **142**, 4168–4179 (2015).
72. Watanave, M. et al. Pharmacological enhancement of retinoid-related orphan receptor alpha function mitigates spinocerebellar ataxia type 3 pathology. *Neurobiol. Dis.* **121**, 263–273 (2019).
73. Huisken, J. & Stainier, D. Y. Even fluorescence excitation by multidirectional selective plane illumination microscopy (mSPIM). *Opt. Lett.* **32**, 2608–2610 (2007).

Author contributions

H.R.U., K.M., T.T.M. and S.A.H. designed the study. T.C.M. developed the CUBIC-X protocols. J.K., T.T.M., T.M. and T.M.W. designed and constructed a customized LSFM. K.M. and T.T.M. developed the MOVIE system. T.M., T.C.M. and S.A.H. prepared the CUBIC-Atlas and analysis programs. H.F. and T.C.M. performed tissue clearing. A.K. and H.H. prepared AAV-PHP.eB (NSE-H2B-mCherry) and the infected mouse. K.M., T.T.M., S.A.H., T.C.M., T.M. and H.R.U. wrote the manuscript. All authors discussed the results and commented on the manuscript text.

Competing interests

H.R.U. and T.C.M. have filed a patent application (PCT/JP2014/070618, 2013-168705) for the CUBIC protocol.

Additional information

Supplementary information is available for this paper at https://doi.org/10.1038/s41596-019-0240-9.

Reprints and permissions information is available at www.nature.com/reprints.

Correspondence and requests for materials should be addressed to H.R.U.

Peer review information *Nature Protocols* thanks Ludovic Silvestri and other anonymous reviewer(s) for their contribution to the peer review of this work.

Publisher's note Springer Nature remains neutral with regard to jurisdictional claims in published maps and institutional affiliations.

Related links
Key references using this protocol
Murakami, T. C. et al. *Nat. Neurosci.* **21**, 625–637 (2018): https://doi.org/10.1038/s41593-018-0109-1
Tainaka, K. et al. *Cell Rep.* **24**, 2196–2210.e9 (2018): https://doi.org/10.1016/j.celrep.2018.07.056
Kubota, S. I. et al. *Cell Rep.* **20**, 236–250 (2017): https://doi.org/10.1016/j.celrep.2017.06.010

Corresponding author(s): Hiroki R. Ueda

Last updated by author(s): May 8, 2019

Reporting Summary

Nature Research wishes to improve the reproducibility of the work that we publish. This form provides structure for consistency and transparency in reporting. For further information on Nature Research policies, see Authors & Referees and the Editorial Policy Checklist.

Statistics

For all statistical analyses, confirm that the following items are present in the figure legend, table legend, main text, or Methods section.

n/a	Confirmed	
☐	☒	The exact sample size (n) for each experimental group/condition, given as a discrete number and unit of measurement
☐	☒	A statement on whether measurements were taken from distinct samples or whether the same sample was measured repeatedly
☒	☐	The statistical test(s) used AND whether they are one- or two-sided *Only common tests should be described solely by name; describe more complex techniques in the Methods section.*
☒	☐	A description of all covariates tested
☒	☐	A description of any assumptions or corrections, such as tests of normality and adjustment for multiple comparisons
☒	☐	A full description of the statistical parameters including central tendency (e.g. means) or other basic estimates (e.g. regression coefficient) AND variation (e.g. standard deviation) or associated estimates of uncertainty (e.g. confidence intervals)
☒	☐	For null hypothesis testing, the test statistic (e.g. F, t, r) with confidence intervals, effect sizes, degrees of freedom and P value noted *Give P values as exact values whenever suitable.*
☒	☐	For Bayesian analysis, information on the choice of priors and Markov chain Monte Carlo settings
☒	☐	For hierarchical and complex designs, identification of the appropriate level for tests and full reporting of outcomes
☒	☐	Estimates of effect sizes (e.g. Cohen's d, Pearson's r), indicating how they were calculated

Our web collection on statistics for biologists contains articles on many of the points above.

Software and code

Policy information about availability of computer code

Data collection	LabVIEW, Visual Studio C# and Andor Solis were used for imaging procedure.
Data analysis	Python, ANTs, Imaris, Visual Studio C#, Microsoft excel and Image J were used. We used custom scripts for counting cells, autofocus simulation and mapping on CUBIC-Atlas.

For manuscripts utilizing custom algorithms or software that are central to the research but not yet described in published literature, software must be made available to editors/reviewers. We strongly encourage code deposition in a community repository (e.g. GitHub). See the Nature Research guidelines for submitting code & software for further information.

Data

Policy information about availability of data

All manuscripts must include a data availability statement. This statement should provide the following information, where applicable:
- Accession codes, unique identifiers, or web links for publicly available datasets
- A list of figures that have associated raw data
- A description of any restrictions on data availability

The data that support the findings of this study are available from the corresponding author upon reasonable request.

Field-specific reporting

Please select the one below that is the best fit for your research. If you are not sure, read the appropriate sections before making your selection.

☒ Life sciences   ☐ Behavioural & social sciences   ☐ Ecological, evolutionary & environmental sciences

Life sciences study design

All studies must disclose on these points even when the disclosure is negative.

Sample size	The sample sizes were determined based on the literatures in the fields. Statistics were not used to predetermine sample sizes.
Data exclusions	We excluded the unannotated cells data from Figure 5e and 5f, because some regions were damaged and distorted during dissection so that cells in these regions were not annotated.
Replication	These protocols were repeated and the results were reliably reproduced. Tissue-clearing, imaging, cell counting and annotation procedures were performed in three mice brains.
Randomization	The mice used for whole-brain cell counting were randomly chosen from colonies.
Blinding	No blinding was done in this study because knowledge of experimental conditions was required during data collection.

Reporting for specific materials, systems and methods

We require information from authors about some types of materials, experimental systems and methods used in many studies. Here, indicate whether each material, system or method listed is relevant to your study. If you are not sure if a list item applies to your research, read the appropriate section before selecting a response.

Materials & experimental systems

n/a	Involved in the study
☒	☐ Antibodies
☒	☐ Eukaryotic cell lines
☒	☐ Palaeontology
☐	☒ Animals and other organisms
☒	☐ Human research participants
☒	☐ Clinical data

Methods

n/a	Involved in the study
☒	☐ ChIP-seq
☒	☐ Flow cytometry
☒	☐ MRI-based neuroimaging

Animals and other organisms

Policy information about studies involving animals; ARRIVE guidelines recommended for reporting animal research

Laboratory animals	8-week-old male mice of C57/BL6 mice were used to analyze whole-brain cell profiling and AAV infection experiment.
Wild animals	N/A
Field-collected samples	N/A
Ethics oversight	N/A

Note that full information on the approval of the study protocol must also be provided in the manuscript.